Integral Sliding Mode Observer Based Disturbance Estimation for Euler-Lagrangian Systems

Zengjie Zhang, Marion Leibold, and Dirk Wollherr, *Senior Member, IEEE*

***Abstract*—In this paper, a novel integral sliding mode observer is proposed to estimate the external disturbance and velocity of Euler-Lagrangian systems. This method provides high bandwidth and precise estimation with only commanded input and position measurement. A system velocity measurement is not required to construct the sliding mode manifold. The convergence of the estimation error to zero is theoretically in finite time, which is proved by a direct Lyapunov method utilizing the passivity property of Euler-Lagrangian systems. An integral sliding manifold is designed to reduce the reaching phase, such that the robustness of the estimation is enhanced. The method has been applied to a robot manipulator to estimate the joint velocity and external contact forces in a physical human-robot task. Simulations and experiments reveal that this novel method provides fast, precise and robust estimation results and can be used to replace the measurement of an external force sensor. The successful application of this observer to a force-sensor-less admittance controller for a manipulator contributes to the implementation of a sensor-free safety framework for human-robot collaboration.**

***Index Terms*—sliding mode observer, fault detection and isolation, human robot interaction, robust control, disturbance estimation.**

I. Introduction

THIS paper is concerned with disturbance estimation and fault detection and isolation (FDI) of mechatronic systems using analytical redundancy based methods. Specifically, it focuses on the online estimation of system actuator faults [1]–[3], external disturbances or forces [4], [5], parametric perturbations [6] and unmodeled system dynamics [7], [8] of a class of Euler-Lagrangian systems which usually share similar mathematical formulations [9]. It is well known that the analysis and diagnosis of fault signals or disturbances are critical techniques of FDI technology. For example, in human-robot interaction (HRI), it is important to detect and classify collisions and contacts to guarantee safety in collaborative tasks [10], [11], such that robots and humans are allowed to share the same workspace and physical injuries are avoided [12]–[14]. More generally, disturbance estimation is also popularly studied for feed-forward disturbance compensation control [8], [15], robust control [16], [17] or fault-tolerant control [18], [19] strategies for various mechatronic systems.

Disturbances like contact forces between robots and the environment can be measured by extrinsic force sensors [11], [20]. However, most other types of disturbances mentioned above are not directly measurable and thus need to be estimated to achieve effective fault diagnosis or compensative control strategies. As a popular approach, the disturbance estimation methods based on the observer theory also referred to as analytic redundancy based methods, are frequently used to solve FDI problems [21], especially the collision detection problem of robotic systems [5], [22]. Since no extrinsic force sensors are needed, these methods are expected to replace real force sensors in HRI tasks to achieve a sensor-less safety framework, thus bring down the cost of the robot system.

Previous work on disturbance estimation of linear systems and Euler-Lagrangian systems is vast, such as unknown input-output observer [23], nonlinear disturbance observer [24], [25], Luenberger observer [26], [27], sliding mode observers [28]–[31], high gain observer [32], filter-based observer [33] and general momentum observers [9]. However, several problems or challenges still exist in these methods. First of all, the Lipschitz condition, which is a basic assumption for some previous methods [32], does not hold for practical mechatronic systems due to the existence of discontinuous friction. Second, the assumption that the derivative of the disturbance is equal to zero, which has been used in previous literature [3], [34], is not general enough to cover high-bandwidth disturbance. Third, since the position is usually the only available measurement in practice, a disturbance estimation method should not rely on velocity measurements. Instead, the velocity of the system should be estimated at the same time [35]–[37]. A precise velocity estimation is important to reconstruct the disturbance estimation [29].

Among the methods above, sliding mode observers solved these three problems, since they do not require the Lipschitz condition nor the disturbance derivative assumption, and they provide robust and *exact* estimation of the velocity (opposite to asymptotic). Specifically, during the sliding motion of a sliding mode observer, the state estimation is invariant from external disturbances (known as *invariance*), and the convergence of the estimation error is in finite time (known as *exact* observation) [35], [36]. Thus the robust precision of state and disturbance estimation is guaranteed [29]. However, the invariance does not hold during the reaching phase to the sliding manifold, which means the traditional sliding mode observers are not always robust. This problem can be solved by the integral sliding mode which can theoretically eliminate the reaching phase, such that the invariance holds from the initial time instance and robustness is enhanced [38]. Even though integral sliding mode controllers are widely studied [39], [40], there has not been related work on the integral sliding mode observer for disturbance estimation of Euler-Lagrangian

This work was supported in part by the China Scholarship Council under Grant 201506120029.

The authors are with Chair of Automatic Control Engineering, Technical University of Munich, 80333, Munich, Germany (e-mail: zengjie.zhang@tum.de; marion.sobotka@tum.de; dw@tum.de).

systems to our knowledge, whereas this enhanced robustness is worthwhile to be investigated in the fields of FDI of HRI.

The contribution of this paper is to propose a novel integral sliding mode observer for velocity and disturbance estimation of Euler-Lagrangian systems. Different from the conventional integral sliding mode based methods applied to disturbance resistance problems [41]–[43], the construction of the switching manifold in this paper does not require the system velocity which is usually not directly measurable in practice. On the contrary, the observer provides fast and precise estimations of the velocity and disturbance of the system simultaneously using only position measurements. There are four advantages to this method. 1) Chattering is reduced since the noisy velocity measurement is not used in the sliding manifold design; 2). A smooth velocity estimation is obtained simultaneously with the disturbance estimation; 3). By applying the idea of integral sliding mode control [38], the reaching phase to the integral sliding manifold is reduced, such that the robustness is enhanced compared to other sliding mode observers; 4). There are no assumptions on the derivative of the system disturbance, which allows the method to be generalizable to a wider range of systems.

The paper is organized as follows. Section II briefly introduces the basic idea of integral sliding mode control and the disturbance estimation problem. The design of the integral sliding mode based observer is discussed in section III along with a finite-time stability proof. In section IV, a simulation is presented to show the feasibility of the integral sliding mode observer, and experiments are conducted in section V to demonstrate its performance in practical applications. Finally, section VI concludes the paper.

II. Preliminaries

A. Integral Sliding Mode Control

This section gives a short introduction of the theory of integral sliding mode [38]. Consider a multi-input multi-output (MIMO) control affine system

$$\dot{\boldsymbol{x}} = \boldsymbol{f}(\boldsymbol{x}) + \boldsymbol{G}(\boldsymbol{x})\left(\boldsymbol{u} + \boldsymbol{d}(\boldsymbol{x},t)\right), \tag{1}$$

where $\boldsymbol{x}(t) \in \mathbb{R}^n$ is the state vector of the system, $\boldsymbol{f}(\boldsymbol{x}) \in \mathbb{R}^n$ is a smooth vector field, $\boldsymbol{G}(\boldsymbol{x}) \in \mathbb{R}^{n\times m}$ is a m-rank smooth matrix, $\boldsymbol{u}(t) = [u_1,\ u_2,\ \cdots,\ u_m]^T$ is the m-dimensional input vector, and $\boldsymbol{d}(\boldsymbol{x},t) \in \mathbb{R}^m$ is the state and time dependent system disturbance which is assumed to be bounded by

$$\|\boldsymbol{d}(\boldsymbol{x},t)\| \leqslant \delta_d,\ \ \delta_d \in \mathbb{R}^+.$$

Note that all norms $\|\cdot\|$ in this paper denote 2-norms. For system (1), an integral sliding mode controller that guarantees the asymptotic stability of the of the equilibrium $\boldsymbol{x} = 0$ is designed as

$$\boldsymbol{u}(t) = \boldsymbol{u}_n + \boldsymbol{u}_s, \tag{2}$$

where $\boldsymbol{u}_n$ is a controller that stabilizes the nominal system and $\boldsymbol{u}_s$ is the discontinuous control input that compensates for the disturbance $\boldsymbol{d}\left(\boldsymbol{x},t\right)$

$$\boldsymbol{u}_s = -M_s\frac{\boldsymbol{s}(\boldsymbol{x},t)}{\|\boldsymbol{s}(\boldsymbol{x},t)\|}, \tag{3}$$

where $M_s \in \mathbb{R}^+$ is a properly selected input gain and the switching function, and

$$\boldsymbol{s}(\boldsymbol{x},t) = \boldsymbol{s}^*(\boldsymbol{x}) + \boldsymbol{z}(t) \tag{4}$$

is the sum of a conventional sliding manifold $\boldsymbol{s}^*(\boldsymbol{x}) \in \mathbb{R}^n$ and an additional integral term $\boldsymbol{z}(t) \in \mathbb{R}^n$, where $\boldsymbol{s}^*(\boldsymbol{x})$ and $\boldsymbol{z}(t)$ respectively satisfy

$$\operatorname{rank}\left(\frac{\partial \boldsymbol{s}^*(\boldsymbol{x})}{\partial \boldsymbol{x}}\right) = m$$

and

$$\dot{\boldsymbol{z}} = -\frac{\partial \boldsymbol{s}^*(\boldsymbol{x})}{\partial \boldsymbol{x}}\left(\boldsymbol{f}(\boldsymbol{x}) + \boldsymbol{G}(\boldsymbol{x})\boldsymbol{u}_n\right),\ \ \boldsymbol{z}(0) = -\boldsymbol{s}^*(\boldsymbol{x}(0))\,,$$

where $\boldsymbol{x}(0)$ is the initial condition of the system state. Note that the control in (3) is referred to as *unit vector control* [35] and guarantees the following sliding mode condition

$$\boldsymbol{s}(\boldsymbol{x},t) = 0,\ \forall\ t \geqslant 0. \tag{5}$$

As a result, the system state $\boldsymbol{x}$ is confined to the sliding manifold (4), and the equivalent sliding mode dynamics is

$$\dot{\boldsymbol{x}} = \boldsymbol{f}(\boldsymbol{x}) + \boldsymbol{G}(\boldsymbol{x})\boldsymbol{u}_n$$

which does not depend on the system disturbance $\boldsymbol{d}(\boldsymbol{x},t)$, if $\boldsymbol{d}(\boldsymbol{x},t)$ is matched [44] as in (1). This feature has been called *invariance* in sliding mode control, since the system behavior is invariant to $\boldsymbol{d}(\boldsymbol{x},t)$. Different from the conventional sliding mode control, integral sliding mode control can theoretically eliminate the reaching phase to the sliding manifold of the system. As a result, the invariance of integral sliding mode control holds for all times.

B. Problem Formulation

The disturbance estimation problem investigated in this paper is formulated as follows. Consider an n-degree-of-freedom (DOF) Euler-Lagrangian system

$$\boldsymbol{M}(\boldsymbol{q})\ddot{\boldsymbol{q}} + \boldsymbol{C}(\boldsymbol{q},\dot{\boldsymbol{q}})\dot{\boldsymbol{q}} + \boldsymbol{G}(\boldsymbol{q}) + \boldsymbol{F}(\dot{\boldsymbol{q}}) = \boldsymbol{\tau} + \boldsymbol{d}_{\text{ext}}(\boldsymbol{q},t), \tag{6}$$

where $\boldsymbol{q}(t) \in \mathbb{R}^n$ is the vector of the generalized coordinates, $\boldsymbol{M}(\boldsymbol{q}) \in \mathbb{R}^{n\times n}$, $\boldsymbol{C}(\boldsymbol{q},\dot{\boldsymbol{q}}) \in \mathbb{R}^{n\times n}$, $\boldsymbol{G}(\boldsymbol{q}) \in \mathbb{R}^n$ and $\boldsymbol{F}(\dot{\boldsymbol{q}}) \in \mathbb{R}^n$ are respectively the inertia matrix, Coriolis and centrifugal matrix, gravitational and frictional vectors. Note that $\boldsymbol{F}(\dot{\boldsymbol{q}})$ usually has a complicated form and contains kinematic discontinuities. $\boldsymbol{\tau} \in \mathbb{R}^n$ is the commanded input, and $\boldsymbol{d}_{\text{ext}}(\boldsymbol{q},t)$ is the external disturbance to the system. In the case of HRI, $\boldsymbol{d}_{\text{ext}}(\boldsymbol{q},t)$ represents the effect of an external contact force in the joint space of a robot manipulator, which is also referred as the external torque [45]. In practice, $\boldsymbol{d}_{\text{ext}}$ can be measured by shaft torque sensors installed on the robot joints. In this paper, the integral sliding mode techniques are applied to estimate $\boldsymbol{d}_{\text{ext}}$ without any extrinsic force sensors.

By defining state variables as

$$\boldsymbol{x}_1 = \boldsymbol{q},\ \ \boldsymbol{x}_2 = \dot{\boldsymbol{q}}, \tag{7}$$

the second order system (6) can be written in state-space form

$$\begin{aligned}\dot{\boldsymbol{x}}_1 &= \boldsymbol{x}_2\\ \dot{\boldsymbol{x}}_2 &= \boldsymbol{M}^{-1}(\boldsymbol{x}_1)\left(\boldsymbol{\tau} - \boldsymbol{C}(\boldsymbol{x}_1,\boldsymbol{x}_2)\boldsymbol{x}_2 - \boldsymbol{G}(\boldsymbol{x}_1) - \boldsymbol{F}(\boldsymbol{x}_2)\right)\\ &\quad + \boldsymbol{d}(\boldsymbol{x}_1,t),\end{aligned} \tag{8}$$

where

$$\boldsymbol{d}(\boldsymbol{x}_1,t)=\boldsymbol{M}^{-1}(\boldsymbol{x}_1)\boldsymbol{d}_{\mathrm{ext}}(\boldsymbol{x}_1,t) \tag{9}$$

is the disturbance of the system to be estimated. Note that in general, the system position $\boldsymbol{x}_1$ is directly measurable by intrinsic sensors like encoders whereas the system velocity $\boldsymbol{x}_2$ is not. In practice, $\boldsymbol{x}_2$ is usually obtained by taking the derivative of $\boldsymbol{x}_1$ and noise is involved. Therefore, the target of this paper is to design an observer for the system (8) to simultaneously estimate the velocity $\hat{\boldsymbol{x}}_2$ and the disturbance $\hat{\boldsymbol{d}}(\boldsymbol{x}_1,t)$ only using the position measurement $\boldsymbol{x}_1$.

C. Properties and Assumptions

For the Euler-Lagrangian system (6), it is well known that the following properties hold.

Property 1. *[46]. The inertia matrix $\boldsymbol{M}(\boldsymbol{x}_1)$ is positive definite and its eigenvalues are bounded by*

$$m_o\leqslant\lambda_M^i(\boldsymbol{x}_1)\leqslant m_O,\ m_o,m_O\in\mathbb{R}^+, \tag{10}$$

where $\lambda_M^i(\boldsymbol{x}_1)$, $i=1,2,\cdots,n$, is the i-th eigenvalue of the inertia matrix $\boldsymbol{M}(\boldsymbol{x}_1)$, and m_o, m_O are respectively the minimal and maximal eigenvalues of $\boldsymbol{M}(\boldsymbol{x}_1)$ over all possible configurations $\boldsymbol{x}_1$, i.e.,

$$m_o=\inf_{\boldsymbol{x}_1}\min_{1\leqslant i\leqslant n}\lambda_M^i(\boldsymbol{x}_1),\ m_O=\sup_{\boldsymbol{x}_1}\max_{1\leqslant i\leqslant n}\lambda_M^i(\boldsymbol{x}_1).$$

Property 2. *[46]. The Coriolis and centrifugal matrix $\boldsymbol{C}(\boldsymbol{x}_1,\boldsymbol{x}_2)$ is bounded by*

$$\|\boldsymbol{C}(\boldsymbol{x}_1,\boldsymbol{x}_2)\|\leqslant c_O\|\boldsymbol{x}_2\|,\ c_O\in\mathbb{R}^+. \tag{11}$$

Property 3. *[46]. The gravity vector is bounded by*

$$\|\boldsymbol{G}(\boldsymbol{x}_1)\|\leqslant g_O,\ g_O\in\mathbb{R}^+.$$

Property 4. *[46]. The matrix $\dot{\boldsymbol{M}}(\boldsymbol{x}_1)-2\boldsymbol{C}(\boldsymbol{x}_1,\boldsymbol{x}_2)$ is skew-symmetric, i.e.,*

$$\boldsymbol{z}^T\left(\dot{\boldsymbol{M}}(\boldsymbol{x}_1)-2\boldsymbol{C}(\boldsymbol{x}_1,\boldsymbol{x}_2)\right)\boldsymbol{z}=0,\ \forall\boldsymbol{z}\in\mathbb{R}^n,$$

where $\dot{\boldsymbol{M}}(\boldsymbol{x}_1)=\mathrm{d}\boldsymbol{M}(\boldsymbol{x}_1)/\mathrm{d}t$ denotes the time derivative of $\boldsymbol{M}(\boldsymbol{x}_1)$.

Property 5. *[28]. The Coriolis and centrifugal matrix $\boldsymbol{C}(\boldsymbol{x}_1,\cdot)$ satisfies*

$$\boldsymbol{C}(\boldsymbol{x}_1,\boldsymbol{\alpha})\boldsymbol{\beta}=\boldsymbol{C}(\boldsymbol{x}_1,\boldsymbol{\beta})\boldsymbol{\alpha},\ \forall\boldsymbol{\alpha},\boldsymbol{\beta}\in\mathbb{R}^n.$$

Assumption 1. *The kinetic energy of the system is bounded, i.e.,*

$$K(\boldsymbol{x}_1,\boldsymbol{x}_2)=\boldsymbol{x}_2^T\boldsymbol{M}(\boldsymbol{x}_1)\boldsymbol{x}_2\leqslant K_O,\ K_O\in\mathbb{R}^+. \tag{12}$$

Corollary 1. *Using Assumption 1, the system velocity $\boldsymbol{x}_2$ is bounded by*

$$\|\boldsymbol{x}_2\|\leqslant\sqrt{K_O/m_o}.$$

Proof. Define $\boldsymbol{L}_M(\boldsymbol{x}_1)$ as the Cholesky decomposition of $\boldsymbol{M}(\boldsymbol{x}_1)$,

$$\boldsymbol{L}_M^T(\boldsymbol{x}_1)\boldsymbol{L}_M(\boldsymbol{x}_1)=\boldsymbol{M}(\boldsymbol{x}_1). \tag{13}$$

Applying Assumption 1 we have

$$(\boldsymbol{L}_M(\boldsymbol{x}_1)\boldsymbol{x}_2)^T\boldsymbol{L}_M(\boldsymbol{x}_1)\boldsymbol{x}_2=\boldsymbol{x}_2^T\boldsymbol{M}(\boldsymbol{x}_1)\boldsymbol{x}_2\leqslant K_O,$$

which leads to $\|\boldsymbol{L}_M(\boldsymbol{x}_1)\boldsymbol{x}_2\|\leqslant\sqrt{K_O}$. Thus,

$$\|\boldsymbol{x}_2\|\leqslant\sqrt{K_O}/\sigma_{\min}(\boldsymbol{L}_M)=\sqrt{K_O/m_o}, \tag{14}$$

where $\sigma_{\min}(\boldsymbol{L}_M)=\sqrt{m_o}$ is the minimal singular value of $\boldsymbol{L}_M(\boldsymbol{x}_1)$ among all $\boldsymbol{x}_1$. □

Assumption 2. *The system disturbance $\boldsymbol{d}(\boldsymbol{x}_1,t)$ is bounded by*

$$\|\boldsymbol{d}(\boldsymbol{x}_1,t)\|\leqslant d_O,\ d_O\in\mathbb{R}^+. \tag{15}$$

Remark 1. *Assumption 1 and 2 are based on the widely accepted assumptions that the kinetic energy and environmental stiffness are finite in practice. Note that in this paper, there are no assumptions on the derivative of $\boldsymbol{d}(\boldsymbol{x}_1,t)$, which allows the work in this paper to be applied to a wider class of systems compared to previous methods in [3], [32], [34].*

III. Observer Design

A. Observer Formulation

The integral sliding mode observer proposed in this paper for disturbance estimation of system (8) is designed as

$$\begin{aligned}\dot{\hat{\boldsymbol{x}}}_1=&\hat{\boldsymbol{x}}_2-\boldsymbol{\Gamma}_1(\hat{\boldsymbol{x}}_1-\boldsymbol{x}_1)+\boldsymbol{u}_1,\\ \dot{\hat{\boldsymbol{x}}}_2=&\hat{\boldsymbol{M}}^{-1}(\boldsymbol{x}_1)\Big(\boldsymbol{\tau}-\hat{\boldsymbol{C}}(\boldsymbol{x}_1,\hat{\boldsymbol{x}}_2)\hat{\boldsymbol{x}}_2-\hat{\boldsymbol{G}}(\boldsymbol{x}_1)-\hat{\boldsymbol{F}}(\hat{\boldsymbol{x}}_2)\Big)\\ &+\boldsymbol{\Gamma}_2\boldsymbol{u}_1+\boldsymbol{u}_2,\end{aligned} \tag{16}$$

where $\hat{\boldsymbol{x}}_1$, $\hat{\boldsymbol{x}}_2$ are the estimated system states, $\hat{\boldsymbol{M}}(\boldsymbol{x}_1)$, $\hat{\boldsymbol{C}}(\boldsymbol{x}_1,\hat{\boldsymbol{x}}_2)$, $\hat{\boldsymbol{G}}(\boldsymbol{x}_1)$ are respectively the identified system parameters, $\boldsymbol{\Gamma}_1\in\mathbb{R}^{n\times n}$ and $\boldsymbol{\Gamma}_2\in\mathbb{R}^{n\times n}$ are positive definite matrices to be determined, and $\boldsymbol{u}_1$ and $\boldsymbol{u}_2$ are the observer inputs respectively defined as

$$\begin{aligned}\boldsymbol{u}_1(t)&=-\alpha_s\frac{\boldsymbol{e}_1(t)}{\|\boldsymbol{e}_1(t)\|}-(\varrho_s+\|\hat{\boldsymbol{x}}_2(t)\|)\frac{\boldsymbol{s}(t)}{\|\boldsymbol{s}(t)\|},\\ \boldsymbol{u}_2(t)&=\epsilon_s\frac{\boldsymbol{u}_1(t)}{\|\boldsymbol{u}_1(t)\|},\end{aligned} \tag{17}$$

where α_s, ϱ_s, $\epsilon_s\in\mathbb{R}^+$ are constants to be determined, $\boldsymbol{e}_1$ denotes the estimation error defined as $\boldsymbol{e}_1=\hat{\boldsymbol{x}}_1-\boldsymbol{x}_1$, and the switching function $\boldsymbol{s}(t)$ is defined as

$$\boldsymbol{s}(t)=\boldsymbol{e}_1(t)+\int_0^t\left(\alpha_s\frac{\boldsymbol{e}_1(\tau)}{\|\boldsymbol{e}_1(\tau)\|}+\boldsymbol{\Gamma}_1\boldsymbol{e}_1(\tau)\right)\mathrm{d}\tau-\boldsymbol{e}_1(0), \tag{18}$$

where $\boldsymbol{e}_1(0)=\hat{\boldsymbol{x}}_1(0)-\boldsymbol{x}_1(0)$ is the initial value of the estimation error. In this sense, the nominal control and the discontinuous control terms $\boldsymbol{u}_n$ and $\boldsymbol{u}_s$ of the observer in (16) corresponding to (2) are respectively

$$\boldsymbol{u}_n=\begin{bmatrix}-\boldsymbol{\Gamma}_1\boldsymbol{e}_1\\ \boldsymbol{0}\end{bmatrix},\ \boldsymbol{u}_s=\begin{bmatrix}\boldsymbol{u}_1\\ \boldsymbol{\Gamma}_2\boldsymbol{u}_1+\boldsymbol{u}_2\end{bmatrix}, \tag{19}$$

where $\boldsymbol{u}_n$ is the nominal continuous feedback input and $\boldsymbol{u}_s$ is the discontinuous input.

For convenience we also define the state estimation error $\boldsymbol{e}_2=\hat{\boldsymbol{x}}_2-\boldsymbol{x}_2$, where $\hat{\boldsymbol{x}}_2$ is the observed velocity. Combining the dynamics of the system (8) and the observer (16), we obtain the dynamics of the estimation errors $\boldsymbol{e}_1$ and $\boldsymbol{e}_2$ as

$$\begin{aligned}\dot{\boldsymbol{e}}_1=&-\boldsymbol{\Gamma}_1\boldsymbol{e}_1+\boldsymbol{e}_2+\boldsymbol{u}_1\\ \dot{\boldsymbol{e}}_2=&-\boldsymbol{M}^{-1}(\boldsymbol{x}_1)\left(\boldsymbol{C}(\boldsymbol{x}_1,\boldsymbol{x}_2)+\boldsymbol{C}(\boldsymbol{x}_1,\hat{\boldsymbol{x}}_2)\right)\boldsymbol{e}_2\\ &+\boldsymbol{\Gamma}_2\boldsymbol{u}_1+\boldsymbol{u}_2-\boldsymbol{d}(\boldsymbol{x}_1,t)-\boldsymbol{h}(\boldsymbol{x}_1,\hat{\boldsymbol{x}}_2),\end{aligned} \tag{20}$$

where $\boldsymbol{h}(\boldsymbol{x}_1, \hat{\boldsymbol{x}}_2)$ is the system uncertainty caused by an inaccurate system identification, see Appendix. Note that the solution of $\boldsymbol{e}_1$ and $\boldsymbol{e}_2$ is in the sense of Filippov but not Lipschitz [35], since (20) contains discontinuous inputs.

Assumption 3. *The system uncertainty $\boldsymbol{h}(\boldsymbol{x}_1, \hat{\boldsymbol{x}}_2)$ is bounded by*

$$\|\boldsymbol{h}(\boldsymbol{x}_1, \hat{\boldsymbol{x}}_2)\| \leqslant h_O \ll d_O,\ h_O \in \mathbb{R}^+. \tag{21}$$

Remark 2. *If the system uncertainty is far smaller than the system disturbance, then $\boldsymbol{h}(\boldsymbol{x}_1, \hat{\boldsymbol{x}}_2)$ can be ignored. This can be achieved by precise system identification.*

According to the sliding mode equivalent control theory in [29], [35], if the disturbance observer (16) is designed in a way that the state estimation errors $\boldsymbol{e}_1$ and $\boldsymbol{e}_2$ in (20) converge to zero equilibrium *in finite time*, i.e.,

$$\boldsymbol{e}_1 = \boldsymbol{0},\ \dot{\boldsymbol{e}}_1 = \boldsymbol{0},\ \forall\ t \geqslant t_1, \tag{22a}$$

$$\boldsymbol{e}_2 = \boldsymbol{0},\ \dot{\boldsymbol{e}}_2 = \boldsymbol{0},\ \forall\ t \geqslant t_2, \tag{22b}$$

where $t_1,\ t_2 \in \mathbb{R}$, $0 < t_1,\ t_2 < +\infty$, then it is not difficult to obtain

$$\boldsymbol{u}_{2\mathrm{eq}}(t) = \boldsymbol{d}(\boldsymbol{x}_1, t) + \boldsymbol{h}(\boldsymbol{x}_1, \hat{\boldsymbol{x}}_2), \tag{23}$$

by substituting (22a) and (22b) into (20), where $\boldsymbol{u}_{2\mathrm{eq}}(t)$ is the equivalent control of observer (16) which denotes the continuous effect of the discontinuously switching control $\boldsymbol{u}_2$ in the Filippov sense. Conditions (22a) and (22b) are also referred to as the *dynamics collapse* or *exact convergence* [35]. Therefore, if Assumption 3 holds, the disturbance can be approximately estimated by

$$\hat{\boldsymbol{d}}(\boldsymbol{x}_1, t) \approx \boldsymbol{u}_{2\mathrm{eq}}(t). \tag{24}$$

It will be discussed in Sec. III-B and Sec. III-C, that the integral sliding mode observer, proposed in this paper, ensures the exact convergence of both $\boldsymbol{e}_1$ and $\boldsymbol{e}_2$ in finite time.

Note that $\boldsymbol{u}_{2\mathrm{eq}}(t)$ cannot be computed explicitly but can be approximated by extracting the low-frequency component of $\boldsymbol{u}_2(t)$ using the following low pass filter, i.e.,

$$F(s) = \frac{1}{\tau s + 1} \tag{25}$$

which is frequently used in previous work [30], [35]. Due to the approximation in (24) and the filtering in (25), the obtained $\hat{\boldsymbol{d}}(\boldsymbol{x}_1, t)$ is no longer a precise estimation of the disturbance $\boldsymbol{d}(\boldsymbol{x}_1, t)$, and the larger τ is, the more spectral component is lost. Therefore, a proper τ should be determined according to the practical requirements to guarantee an acceptable precision for the estimation result $\hat{\boldsymbol{d}}(\boldsymbol{x}_1, t)$.

B. Existence of the Sliding Mode Condition

In this section, we investigate the sliding mode condition of the sliding manifold defined as in (5). It will be shown in Sec III-C, that this is a sufficient condition for the finite time stability of the closed-loop system as in (20) at the zero equilibrium.

Theorem 1. *If the sliding manifold in (16) is designed as (18) and the parameter ϱ_s in (17) is selected such that*

$$\varrho_s \geqslant \sqrt{K_O/m_o} + \varrho_0,\ \varrho_0 \in \mathbb{R}^+, \tag{26}$$

where K_O and m_o are respectively defined as in (12) and (10), then the following sliding mode condition holds,

$$\boldsymbol{s}(t) = \boldsymbol{0},\ \dot{\boldsymbol{s}}(t) = \boldsymbol{0},\ \forall\ t > 0. \tag{27}$$

Proof. By defining a Lyapunov function

$$V_s(t) = \frac{1}{2}\boldsymbol{s}(t)^T\boldsymbol{s}(t) \tag{28}$$

and calculating the derivative of $\boldsymbol{s}(t)$ from (18)

$$\dot{\boldsymbol{s}}(t) = \dot{\boldsymbol{e}}_1(t) + \alpha_s\frac{\boldsymbol{e}_1(t)}{\|\boldsymbol{e}_1(t)\|} + \boldsymbol{\Gamma}_1\boldsymbol{e}_1(t), \tag{29}$$

we obtain the derivative of $V_s(t)$ as

$$\dot{V}_s = \boldsymbol{s}^T\dot{\boldsymbol{s}} = \boldsymbol{s}^T\left(\dot{\boldsymbol{e}}_1 + \alpha_s\frac{\boldsymbol{e}_1}{\|\boldsymbol{e}_1\|} + \boldsymbol{\Gamma}_1\boldsymbol{e}_1\right).$$

For $\dot{\boldsymbol{e}}_1$ from (20) and $\boldsymbol{u}_1$ from (17), it follows that

$$\begin{aligned}\dot{V}_s =& \boldsymbol{s}^T\left(\boldsymbol{e}_2 - (\varrho_s + \|\hat{\boldsymbol{x}}_2\|)\frac{\boldsymbol{s}}{\|\boldsymbol{s}\|}\right)\\ =& \boldsymbol{s}^T\boldsymbol{e}_2 - (\varrho_s + \|\hat{\boldsymbol{x}}_2\|)\|\boldsymbol{s}\|\\ \leqslant& \|\boldsymbol{s}\|\|\boldsymbol{e}_2\| - (\varrho_s + \|\hat{\boldsymbol{x}}_2\|)\|\boldsymbol{s}\|\end{aligned}. \tag{30}$$

Since we have

$$\|\boldsymbol{e}_2\| = \|\hat{\boldsymbol{x}}_2 - \boldsymbol{x}_2\| \leqslant \|\hat{\boldsymbol{x}}_2\| + \|\boldsymbol{x}_2\| < \varrho_s + \|\boldsymbol{x}_2\|, \tag{31}$$

(30) leads to

$$\begin{aligned}\dot{V}_s \leqslant& \|\boldsymbol{s}\|\|\hat{\boldsymbol{x}}_2\| + \|\boldsymbol{s}\|\|\boldsymbol{x}_2\| - \varrho_s\|\boldsymbol{s}\| - \|\hat{\boldsymbol{x}}_2\|\|\boldsymbol{s}\|\\ =& -(\varrho_s - \|\boldsymbol{x}_2\|)\sqrt{2V_s}.\end{aligned}$$

Considering Corollary 1 and substituting (26), we have

$$\dot{V}_s \leqslant -\varrho_0\sqrt{2V_s}.$$

Thus, V_s is bounded by

$$0 \leqslant V_s(t) \leqslant V_s^*(t), \tag{32}$$

where

$$V_s^*(t) = \begin{cases} \dfrac{1}{2}\left(\|\boldsymbol{s}(0)\| - \varrho_0 t\right)^2, & 0 \leqslant t < \dfrac{1}{\varrho_s}\|\boldsymbol{s}(0)\|,\\ 0, & t \geqslant \dfrac{1}{\varrho_s}\|\boldsymbol{s}(0)\|.\end{cases}$$

Using (18), we conclude that

$$V_s^*(0) = \frac{1}{2}\boldsymbol{s}^T(0)\boldsymbol{s}(0) = 0,$$

and finally get

$$V_s(t) = V_s^*(t) = 0,\ \forall\ t \geqslant 0. \tag{33}$$

Note that from (32) to (33), the comparison lemma [47] is applied, and $\dot{V}_s(t)$ and $\dot{V}_s^*(t)$ are continuous in the Filippov sense. Therefore, referring to (28), (33) leads to

$$\boldsymbol{s}(t) = 0,\ \forall t \geqslant 0, \tag{34}$$

which indicates a sliding mode of the dynamics (20) from the initial time instant $t = 0$ and the collapsed dynamics of $\boldsymbol{s}(t)$

as in (27) [35]. Note that $\dot{\boldsymbol{s}}(t)$ is also continuous in the sense of Filippov. $\square$

Remark 3. *By designing the switching function (18) in integral form, the reaching phase is theoretically eliminated and the sliding mode exits for all $t \geqslant 0$. Thus, invariance with respect to the disturbance $\mathbf{d}(\boldsymbol{x}_1, t)$ holds for all $t \geqslant 0$. Note that due to the measurement uncertainties, (5) does not strictly hold in practice and the reaching phase is not eliminated but reduced to a minimum compared to the conventional sliding mode methods.*

C. Stability Analysis

In this section, the finite-time convergence of the estimation errors $\boldsymbol{e}_1$ and $\boldsymbol{e}_2$ in (20) to the zero equilibrium is given by the following theorem based on the sliding mode condition (27) ensured by Theorem 1.

Theorem 2. *If the parameters $\boldsymbol{\Gamma}_1$, $\boldsymbol{\Gamma}_2$, α_s and ϵ_s in (16) and (17) are determined such that*

$$\alpha_s > 0,\ \epsilon_s > \epsilon_0 + h_O + d_O, \boldsymbol{\Gamma}_1 > 0,\ \boldsymbol{\Gamma}_2 > \frac{c_O}{m_o}\|\hat{\boldsymbol{x}}_2\|\boldsymbol{I}_n, \quad (35)$$

where $\epsilon_0 \in \mathbb{R}^+$, the boundary scalars m_o, c_O, d_O and h_O are respectively defined in (10), (11), (15) and (21), and $\boldsymbol{I}_n$ is the n-dimensional identity matrix, then $\boldsymbol{e}_1(t)$ and $\boldsymbol{e}_2(t)$ converge to the zero equilibria as in (22a) and (22b) respectively in finite time t_1 and t_2, where $t_1,\ t_2 < +\infty$ are bounded by

$$t_1 < \frac{1}{\alpha_s}\|\boldsymbol{e}_1(0)\|,\ t_2 < t_1 + \frac{1}{\epsilon_s\sqrt{m_o}}\|\bar{\boldsymbol{e}}_2(t_1)\|, \quad (36)$$

where m_o is the minimal eigenvalue of $\boldsymbol{M}(\boldsymbol{x}_1)$ as in (10), and $\bar{\boldsymbol{e}}_2(t)$ is defined as

$$\bar{\boldsymbol{e}}_2(t) = \boldsymbol{L}_M(\boldsymbol{x}_1(t))\boldsymbol{e}_2(t), \quad (37)$$

where $\boldsymbol{L}_M$ is the Cholesky matrix of $\boldsymbol{M}(\boldsymbol{x}_1)$ as in (13).

Proof. We define the following Lyapunov function

$$V_e(t) = V_1(t) + V_2(t),$$

where

$$V_1(t) = \frac{1}{2}\boldsymbol{e}_1^T\boldsymbol{e}_1,\ V_2(t) = \frac{1}{2}\boldsymbol{e}_2^T\boldsymbol{M}(\boldsymbol{x}_1)\boldsymbol{e}_2.$$

Considering (27), by differentiating $\boldsymbol{e}_1$ in (20), we obtain

$$\dot{\boldsymbol{e}}_1 = -\alpha_s\frac{\boldsymbol{e}_1}{\|\boldsymbol{e}_1\|} - \boldsymbol{\Gamma}_1\boldsymbol{e}_1, \quad (38)$$

and the derivative of V_1 reads

$$\dot{V}_1 = \boldsymbol{e}_1^T\dot{\boldsymbol{e}}_1 = -\alpha_s\|\boldsymbol{e}_1\| - \boldsymbol{e}_1^T\boldsymbol{\Gamma}_1\boldsymbol{e}_1 < -\alpha_s\sqrt{2V_1}. \quad (39)$$

The solution of the inequality (39) results in $0 \leqslant V_1(t) \leqslant V_1^*(t)$, $\forall\, t \geqslant 0$, where

$$V_1^*(t) = \begin{cases} \frac{1}{2}\left(\|\boldsymbol{e}_1(0)\| - \alpha_s t\right)^2, & 0 \leqslant t < \frac{1}{\alpha_s}\|\boldsymbol{e}_1(0)\|, \\ 0, & t \geqslant \frac{1}{\alpha_s}\|\boldsymbol{e}_1(0)\|, \end{cases}$$

which leads to

$$V_1(t) = 0,\ t \geqslant t_1, \quad (40)$$

where t_1 is confined by

$$t_1 < \frac{1}{\alpha_s}\|\boldsymbol{e}_1(0)\| < +\infty. \quad (41)$$

Similar to the proof of Theorem 1, it can be concluded from (40) that the dynamics of $\boldsymbol{e}_1(t)$ is governed by the algebraic equations (22a), which indicates that the estimation error $\boldsymbol{e}_1(t)$ converges to zero in finite time and the dynamics collapse occurs afterwards. Note that $\dot{V}_1(t)$, $\dot{V}_1^*(t)$ and $\dot{\boldsymbol{e}}_1(t)$ are continuous in the sense of Filippov.

Now we consider the convergence of the velocity estimation error $\boldsymbol{e}_2(t)$. Substituting (20), the time derivative of $V_2(t)$ reads

$$\begin{aligned}\dot{V}_2 =& \boldsymbol{e}_2^T\boldsymbol{M}(\boldsymbol{x}_1)\dot{\boldsymbol{e}}_2 + \frac{1}{2}\boldsymbol{e}_2^T\dot{\boldsymbol{M}}(\boldsymbol{x}_1)\boldsymbol{e}_2 \\ =& -\boldsymbol{e}_2^T(\boldsymbol{C}(\boldsymbol{x}_1, \boldsymbol{x}_2) + \boldsymbol{C}(\boldsymbol{x}_1, \hat{\boldsymbol{x}}_2))\boldsymbol{e}_2 + \boldsymbol{e}_2^T\boldsymbol{M}(\boldsymbol{x}_1)\boldsymbol{\Gamma}_2\boldsymbol{u}_1 \\ & \boldsymbol{e}_2^T\boldsymbol{M}(\boldsymbol{x}_1)\left(\boldsymbol{u}_2 - \boldsymbol{d} - \boldsymbol{h}\right) + \frac{1}{2}\boldsymbol{e}_2^T\dot{\boldsymbol{M}}(\boldsymbol{x}_1)\boldsymbol{e}_2 \\ =& \boldsymbol{e}_2^T\left(\frac{1}{2}\dot{\boldsymbol{M}}(\boldsymbol{x}_1) - \boldsymbol{C}(\boldsymbol{x}_1, \boldsymbol{x}_2)\right)\boldsymbol{e}_2 + \boldsymbol{e}_2^T\boldsymbol{M}(\boldsymbol{x}_1)\boldsymbol{\Gamma}_2\boldsymbol{u}_1 \\ & \boldsymbol{e}_2^T\boldsymbol{M}(\boldsymbol{x}_1)\left(\boldsymbol{u}_2 - \boldsymbol{d} - \boldsymbol{h}\right) - \frac{1}{2}\boldsymbol{e}_2^T\boldsymbol{C}(\boldsymbol{x}_1, \hat{\boldsymbol{x}}_2)\boldsymbol{e}_2\end{aligned} \quad (42)$$

According to Property 4, we have

$$\boldsymbol{e}_2^T\left(\frac{1}{2}\dot{\boldsymbol{M}}(\boldsymbol{x}_1) - \boldsymbol{C}(\boldsymbol{x}_1, \boldsymbol{x}_2)\right)\boldsymbol{e}_2 = 0. \quad (43)$$

Therefore, substituting (17) and (43) to (42), we obtain

$$\begin{aligned}\dot{V}_2 =& \boldsymbol{e}_2^T\boldsymbol{M}(\boldsymbol{x}_1)\boldsymbol{\Gamma}_2\boldsymbol{u}_1 - \frac{1}{2}\boldsymbol{e}_2^T(\boldsymbol{C}(\boldsymbol{x}_1, \hat{\boldsymbol{x}}_2) + \boldsymbol{C}(\boldsymbol{x}_1, \hat{\boldsymbol{x}}_2))\boldsymbol{e}_2 \\ & + \epsilon_s\frac{\boldsymbol{e}_2^T\boldsymbol{M}(\boldsymbol{x}_1)\boldsymbol{u}_1}{\|\boldsymbol{u}_1\|} - \boldsymbol{e}_2^T\boldsymbol{M}(\boldsymbol{x}_1)\left(\boldsymbol{d} + \boldsymbol{h}\right).\end{aligned} \quad (44)$$

Substituting the collapsed dynamics of $\boldsymbol{e}_1$ in (22a) to $\dot{\boldsymbol{e}}_1$ in (20), we have

$$\boldsymbol{0} = \boldsymbol{u}_1 + \boldsymbol{e}_2,\ t \geqslant t_1, \quad (45)$$

which holds in the sense of Filippov. Thus, substituting (45) to (44) we have

$$\begin{aligned}\dot{V}_2 =& -\boldsymbol{e}_2^T\left(\boldsymbol{\Gamma}_2\boldsymbol{M}(\boldsymbol{x}_1) + \frac{1}{2}\boldsymbol{C}^T(\boldsymbol{x}_1, \hat{\boldsymbol{x}}_2) + \frac{1}{2}\boldsymbol{C}(\boldsymbol{x}_1, \hat{\boldsymbol{x}}_2)\right)\boldsymbol{e}_2 \\ & - \epsilon_s\frac{\boldsymbol{e}_2^T\boldsymbol{M}(\boldsymbol{x}_1)\boldsymbol{e}_2}{\|\boldsymbol{e}_2\|} - \boldsymbol{e}_2^T\boldsymbol{M}(\boldsymbol{x}_1)\left(\boldsymbol{d} + \boldsymbol{h}\right).\end{aligned} \quad (46)$$

Considering the selection of $\boldsymbol{\Gamma}_2$ and γ_s in (35), we have

$$\begin{aligned}& \boldsymbol{\Gamma}_2\boldsymbol{M}(\boldsymbol{x}_1) + \frac{1}{2}\boldsymbol{C}^T(\boldsymbol{x}_1, \hat{\boldsymbol{x}}_2) + \frac{1}{2}\boldsymbol{C}(\boldsymbol{x}_1, \hat{\boldsymbol{x}}_2) \\ > & \frac{c_O\|\hat{\boldsymbol{x}}_2\|}{m_o}\boldsymbol{M}(\boldsymbol{x}_1) + \frac{1}{2}\boldsymbol{C}^T(\boldsymbol{x}_1, \hat{\boldsymbol{x}}_2) + \frac{1}{2}\boldsymbol{C}(\boldsymbol{x}_1, \hat{\boldsymbol{x}}_2) \geqslant 0,\end{aligned} \quad (47)$$

where Property 1 and 2 are applied. Therefore, (46) leads to

$$\dot{V}_2 < -\epsilon_s\frac{\boldsymbol{e}_2^T\boldsymbol{M}(\boldsymbol{x}_1)\boldsymbol{e}_2}{\|\boldsymbol{e}_2\|} - \boldsymbol{e}_2^T\boldsymbol{M}(\boldsymbol{x}_1)\left(\boldsymbol{d} + \boldsymbol{h}\right). \quad (48)$$

Substituting (13), we have

$$\begin{aligned}\dot{V}_2 <& -\epsilon_s\frac{\|\boldsymbol{L}_{\mathrm{M}}\boldsymbol{e}_2\|}{\|\boldsymbol{e}_2\|}\frac{\boldsymbol{e}_2^T\boldsymbol{M}(\boldsymbol{x}_1)\boldsymbol{e}_2}{\|\boldsymbol{L}_{\mathrm{M}}\boldsymbol{e}_2\|} - (\boldsymbol{L}_M\boldsymbol{e}_2)^T\boldsymbol{L}_M(\boldsymbol{d} + \boldsymbol{h}) \\ \leqslant& -\epsilon_s\sigma_{\min}(\boldsymbol{L}_M)\left\|\boldsymbol{L}_M\boldsymbol{e}_2\right\| + \|\boldsymbol{L}_M\boldsymbol{e}_2\|\|\boldsymbol{L}_M(\boldsymbol{d} + \boldsymbol{h})\| \\ \leqslant& \left(-\epsilon_s + \|\boldsymbol{d} + \boldsymbol{h}\|\right)\sigma_{\min}(\boldsymbol{L}_M)\left\|\boldsymbol{L}_M\boldsymbol{e}_2\right\|, \\ \leqslant& \left(-\epsilon_s + d_O + h_O\right)\sqrt{m_o}\left\|\boldsymbol{L}_M\boldsymbol{e}_2\right\|,\end{aligned}$$

Considering (35), we obtain

$$\dot{V}_2 < -\epsilon_0 \sqrt{2 m_o V_2}.$$

Thus, $V_2(t)$ is bounded by $0 \leqslant V_2(t) \leqslant V_2^*(t),\ t \geqslant t_1$, where $V_2^*(t) = \frac{1}{2}\left(\|\bar{e}_2(t_1)\| + \epsilon_0\sqrt{m_o}\,(t_1 - t)\right)^2$ for $t_1 \leqslant t < t_1 + \frac{1}{\epsilon_0\sqrt{m_o}}\|\bar{e}_2(t_1)\|$, and $V_2^*(t) = 0$ for $t \geqslant t_1 + \frac{1}{\epsilon_0\sqrt{m_o}}\|\bar{e}_2(t_1)\|$, which leads to

$$V_2(t) = 0,\ t \geqslant t_2, \tag{49}$$

where t_2 is confined by

$$t_2 < t_1 + \frac{1}{\epsilon_0\sqrt{m_o}}\|\bar{e}_2(t_1)\| < +\infty.$$

Therefore, $\boldsymbol{e}_2(t)$ achieves dynamics collapse within finite time t_2. Note that $\dot{V}_2(t)$, $\dot{V}_2^*(t)$ and $\dot{\boldsymbol{e}}_2(t)$ are also continuous in the sense of Filippov. □

Remark 4. *In the proof of Theorem 2, it is noticed that the dynamics collapse of $\boldsymbol{e}_1(t)$ is a necessary condition of the finite-time convergence of $\boldsymbol{e}_2(t)$. Therefore, the sliding mode of $\boldsymbol{e}_2$ is achieved only after the convergence of $\boldsymbol{e}_1$. By constructing such successive sliding modes of $\boldsymbol{s}$, $\boldsymbol{e}_1$ and $\boldsymbol{e}_2$, the proposed observer (16) ensures a theoretically precise estimation of the disturbance $\boldsymbol{d}$ without the velocity measurement $\boldsymbol{x}_2$.*

Different from the conventional integral sliding mode which merely ensures the asymptotic convergence of system states, the proposed observer in (16) guarantees the finite-time convergence of both $\boldsymbol{s}(t)$ and the estimation errors $\boldsymbol{e}_1(t)$ and $\boldsymbol{e}_2(t)$ to zero. Nevertheless, we still name the method as an *integral sliding mode observer*, since it possesses the advantage of conventional integral sliding mode, i.e., the sliding mode is achieved since the initial time instant.

D. Chattering Reduction and Filtering

Similar to the conventional sliding mode controller, chattering is a major issue for this integral sliding mode observer. The main reason for chattering is the finite switching frequency, which is confined by the sampling rate of the system. To reduce the chattering and obtain a smooth disturbance estimation, the boundary layer method is applied in this paper. We change the unit control switching function in (17) into the following modified form

$$\begin{aligned} \boldsymbol{u}_1 &= -\frac{\alpha_s \boldsymbol{e}_1}{\|\boldsymbol{e}_1\| + \delta_e} - (\varrho_s + \|\hat{\boldsymbol{x}}_2(t)\|)\,\frac{\boldsymbol{s}}{\|\boldsymbol{s}\| + \delta_s}, \\ \boldsymbol{u}_2 &= \frac{\epsilon_s \boldsymbol{u}_1}{\|\boldsymbol{u}_1\| + \delta_u}, \end{aligned} \tag{50}$$

and the sliding manifold $\boldsymbol{s}$ from (18) is also modified to

$$\boldsymbol{s} = \boldsymbol{e}_1 + \int_{t_0}^{t}\left(\frac{\alpha_s \boldsymbol{e}_1}{\|\boldsymbol{e}_1\| + \delta_e} + \boldsymbol{\Gamma}_1 \boldsymbol{e}_1\right)\mathrm{d}\tau - \boldsymbol{e}_1(0),$$

where $\delta_{\mathrm{e}},\ \delta_{\mathrm{s}},\ \delta_{\mathrm{u}} \in \mathbb{R}^{+}0$ are scalars that determine the width of the boundary layers.

Note that after applying this modification, the finite-time convergence of $\boldsymbol{s}(t)$, $\boldsymbol{e}_1(t)$ and $\boldsymbol{e}_2(t)$ do not strictly hold with respect to the equilibria as in (27), (22a) and (22b), but only with respect to the boundary layers $\|\boldsymbol{s}(t)\| \leqslant \delta_s$, $\|\boldsymbol{e}_1(t)\| \leqslant \delta_e$ and $\|\boldsymbol{e}_2(t)\| \leqslant \delta_u$ instead. The consequence is inferior estimation precision and robustness. Therefore, a compromise has to be found between estimation performance and the chattering level, and the boundary layer parameters δ_e, δ_s and δ_u should be carefully determined according to the specific requirements of practical applications.

IV. SIMULATION

The proposed integral sliding mode observer has been evaluated by a simulation of a 3-DOF robot manipulator described by (6). In this simulation, we run the robot with a given desired trajectory and a PD tracking controller. A predefined disturbance torque $\boldsymbol{d}_{\mathrm{ext}}$ is exerted on the joints during the motion of the robot. Meanwhile, the integral sliding mode observer is implemented to obtain the online estimation $\hat{\boldsymbol{d}}_{\mathrm{ext}}$. Then, the observer is evaluated based on the comparison between $\boldsymbol{d}_{\mathrm{ext}}$ and $\hat{\boldsymbol{d}}_{\mathrm{ext}}$. The dynamic parameters of the simulated manipulator model are shown in Tab. I and Tab. II, where $m_{ij},\ i,j = 1,2,3$ are the corresponding elements in the inertia matrix $\boldsymbol{M}(\boldsymbol{q})$ and $n_k,\ k = 1,2,3$ are the elements of the Coriolis and centrifugal vector $\boldsymbol{C}(\boldsymbol{q},\dot{\boldsymbol{q}})\dot{\boldsymbol{q}}$. For brevity, the gravity and friction terms are omitted to simulate a frictionless robot confined in the horizontal plane. The values of the parameters are listed in Tab. III and IV, where $q_i, \dot{q}_i \in \mathbb{R}$ respectively denote the angular position and velocity of the i-th joint. The simulation is implemented using a first order Euler solver with sampling rate 1 kHz and runs for 6 s.

TABLE I
ELEMENTS OF INERTIA MATRIX ('VAR' FOR 'VARIABLE')

Var	Expression	Var	Expression
m_{11}	$\alpha_1 + 2\beta_1 c_{23} + 2\beta_2 c_2 + 2\beta_3 c_3$	m_{22}	$\alpha_2 + \beta_3 c_3$
m_{12}	$\alpha_2 + \beta_1 c_{23} + \beta_2 c_2 + 2\beta_3 c_3$	m_{23}	$\alpha_3 + \beta_3 c_3$
m_{13}	$\alpha_3 + \beta_1 c_{23} + \beta_3 c_3$	m_{33}	α_3

TABLE II
ELEMENTS OF CORIOLIS AND CENTRIFUGAL VECTOR

Var	Expression
n_1	$\gamma_1 s_2 \dot{q}_1^2 + \gamma_2 s_{23}\dot{q}_1^2 + \gamma_3 s_2(\dot{q}_1 + \dot{q}_2)^2 + \gamma_4 s_3(\dot{q}_1 + \dot{q}_2)^2$ $+\gamma_5 s_{23}(\dot{q}_1 + \dot{q}_2 + \dot{q}_3)^2 + \gamma_6 s_3(\dot{q}_1 + \dot{q}_2 + \dot{q}_3)^2$
n_2	$\gamma_1 s_2 \dot{q}_1^2 + \gamma_2 s_{23}\dot{q}_1^2 + \gamma_4 s_3(\dot{q}_1 + \dot{q}_2)^2$ $+\gamma_6 s_3(\dot{q}_1 + \dot{q}_2 + \dot{q}_3)^2$
n_3	$\gamma_2 s_{23}\dot{q}_1^2 + \gamma_4 s_3(\dot{q}_1 + \dot{q}_2)^2$

TABLE III
TRIGONOMETRIC FUNCTIONS ('SYM' FOR 'SYMBOL')

Sym	Expression	Sym	Expression	Sym	Expression
c_2	$\cos(q_2)$	c_3	$\cos(q_3)$	c_{23}	$\cos(q_2 + q_3)$
s_2	$\sin(q_2)$	s_3	$\sin(q_3)$	s_{23}	$\sin(q_2 + q_3)$

In the simulation, a sinusoidal desired trajectory $\boldsymbol{q}_d(t) \in \mathbb{R}^3$ in joint space is defined as (see Fig. (1))

$$\boldsymbol{q}_d(t) = \left(1 + \sin\left(\frac{\pi}{3}t - \frac{\pi}{6}\right)\right)\boldsymbol{k}_{\mathrm{pos}},\ 0 \leqslant t \leqslant 6,$$

where $\boldsymbol{k}_{\mathrm{pos}} = [\ 0.5\quad 0.8\quad 0.2\ ]^T$ is the coefficient vector to distribute different amplitudes to each joint. The manipulator

TABLE IV
SYSTEM PARAMETERS ('PAR' FOR 'PARAMETER')

Par	Value	Par	Value	Par	Value	Par	Value
α_1	1.0425	β_1	0.0405	γ_1	0.1742	γ_4	0.0281
α_2	0.4398	β_2	0.1742	γ_2	0.0405	γ_5	-0.0405
α_3	0.1788	β_3	0.0281	γ_3	-0.1742	γ_6	-0.0281

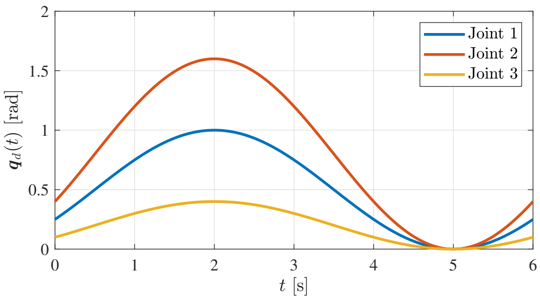

Fig. 1. The desired robot trajectory $\boldsymbol{q}_d(t)$ for simulation.

is configured with non-zero initial conditions, i.e. $\boldsymbol{q}(0) = [\ 0.25 \ \ 0.4 \ \ 0.1\ ]^T$ and $\dot{\boldsymbol{q}}(0) = [\ 0.45 \ \ 0.73 \ \ 0.18\ ]^T$. A PD controller is designed for the robot to track the given trajectory $\boldsymbol{q}_d(t)$,

$$\boldsymbol{\tau} = \boldsymbol{M}(\boldsymbol{q})\left(\ddot{\boldsymbol{q}}_d + \boldsymbol{K}_D\dot{\boldsymbol{e}}_q + \boldsymbol{K}_{\mathrm{P}}\boldsymbol{e}_q\right) + \boldsymbol{C}(\boldsymbol{q},\dot{\boldsymbol{q}})\dot{\boldsymbol{q}}, \tag{51}$$

where $\boldsymbol{e}_q = \boldsymbol{q}_d - \boldsymbol{q}$ and $\dot{\boldsymbol{e}}_q = \dot{\boldsymbol{q}}_d - \dot{\boldsymbol{q}}$ are the tracking errors, $\boldsymbol{K}_{\mathrm{P}} = 200\boldsymbol{I}_3$, $\boldsymbol{K}_d = 36\boldsymbol{I}_3$ are the diagonal proportional and derivative gain matrices, and $\boldsymbol{I}_3$ is a 3×3 unit diagonal matrix.

Sinusoidal disturbance torques $\boldsymbol{d}_{\mathrm{ext}}(t)$ are added to the commanded input $\boldsymbol{\tau}$ on the three joints of the robot in the simulation which are

$$\boldsymbol{d}_{\mathrm{ext}}(t) = \begin{cases} 0, & 0 \leqslant t \leqslant 2.5 \\ \sin\left(\dfrac{\pi}{2}(t-0.5)\right)\boldsymbol{k}_{\mathrm{dst}}, & 0.5 < t \leqslant 2.5, \\ \sin\left(\dfrac{\pi}{2}(t-4)\right)\boldsymbol{k}_{\mathrm{dst}}, & 4 < t \leqslant 6, \end{cases} \tag{52}$$

where $\boldsymbol{k}_{\mathrm{dst}} = [\ 15 \ \ 18 \ \ 12\ ]^T$ is the coefficient vector. Similar disturbances are also used in related work, such as in [3], since they resembles the waveform of contact forces in practice.

An integral sliding mode observer in (16) is implemented to estimate the disturbance $\hat{\boldsymbol{d}}_{\mathrm{ext}}(t)$ in (52). The parameters of the observer are listed in Tab. V. The initial states of the observer are set to $\hat{\boldsymbol{x}}_1(0) = \boldsymbol{0}$ and $\hat{\boldsymbol{x}}_2(0) = \boldsymbol{0}$. The evaluation of the simulation results are as follows. For brevity, only the results of the first joint are displayed, since the results on the three joints are similar.

TABLE V
OBSERVER PARAMETERS

Par	Value	Par	Value	Par	Value	Par	Value
ϵ_s	190	ϱ_s	240	δ_a	0.2	$\boldsymbol{\Gamma}_1$	$112\boldsymbol{I}_3$
α_s	10	δ_s	0.1	δ_u	0.3	$\boldsymbol{\Gamma}_2$	$175\boldsymbol{I}_3$

In Fig. 2a, the original disturbance $\boldsymbol{d}_{\mathrm{ext}}(t)$ and its estimation $\hat{\boldsymbol{d}}_{\mathrm{ext}}(t)$ are compared. It is noticed that, even though the

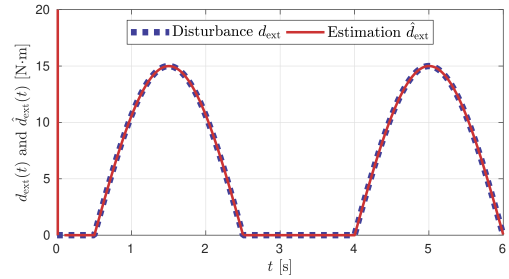

(a) The disturbance $d_{\mathrm{ext}}(t)$ and its estimation $\hat{d}_{\mathrm{ext}}(t)$ of the first joint.

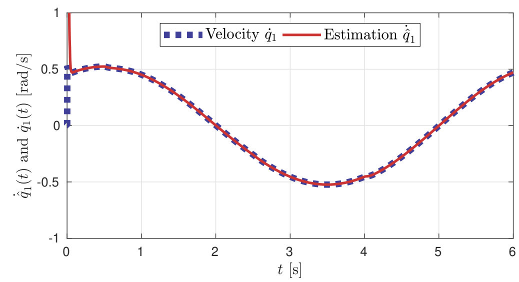

(b) The joint velocity $\dot{q}_1$ and its estimation $\hat{\dot{q}}_1$ of the first joint.

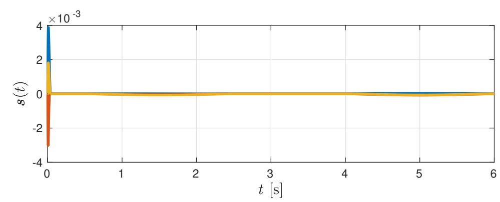

(c) The switching function $\boldsymbol{s}(t)$ indicates the enhanced robustness of the integral sliding mode observer.

Fig. 2. The estimation results for sinusoidal disturbance shows the high precision and bandwidth of the observer.

non-zero initial conditions are given, the estimation $\hat{\boldsymbol{d}}_{\mathrm{ext}}(t)$ precisely tracks $\boldsymbol{d}_{\mathrm{ext}}(t)$ after a short transient stage (approx. 0.0625s), even at the time instants where sharp changes emerge in the disturbance (e.g. 0.5s, 2.5s and 4s). This confirms the high-bandwidth feature of the integral sliding mode observer. Fig. (2b) shows the comparison between the measured velocity $\dot{\boldsymbol{q}}(t)$ and its estimation $\hat{\dot{\boldsymbol{q}}}(t)$ by the observer. Note that the measured velocity comes from the direct derivative of measured position $\boldsymbol{q}(t)$. Similar to the estimation of the disturbance, $\hat{\dot{\boldsymbol{q}}}(t)$ converges to $\dot{\boldsymbol{q}}(t)$ after a short transient stage (also approx 0.0625s). Fig. (2c) shows that the switching function $\boldsymbol{s}(t)$ is kept within the range $\|\boldsymbol{s}(t)\| < 4\times10^{-3}$ despite the non-zero initial condition $\boldsymbol{e}_1(0) = [-0.25 \ \ -0.4 \ \ -0.1]^T$. This result reveals the effectiveness of the proposed integral sliding mode observer that the velocity estimation $\hat{\dot{\boldsymbol{q}}}(t)$ is always invariant from disturbance $\boldsymbol{d}_{\mathrm{ext}}(t)$. Thus, the enhanced robustness of this novel observer is confirmed.

V. EXPERIMENT

In this section, the proposed observer has been applied to a robot platform (see Fig. 3) to evaluate its estimation performance in practice. Similar to the simulation, in this experiment, the robot is actuated by a PD controller tracking

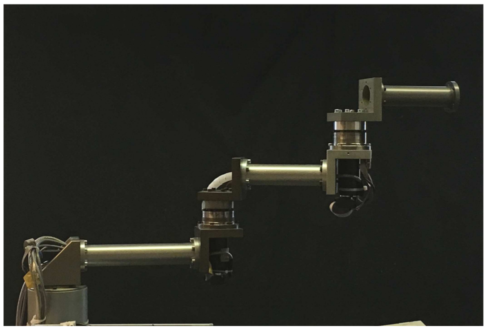

Fig. 3. The 3-DOF robot platform in the experiment.

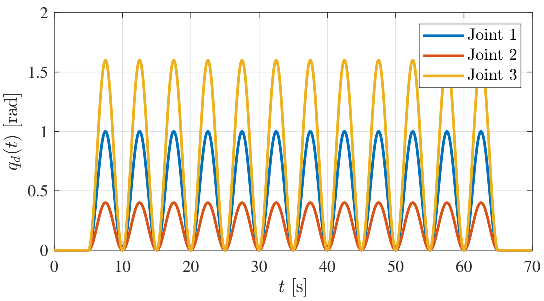

Fig. 4. The desired trajectory for the robot in the experiment.

the given desired trajectory. Different types of disturbance are added to the joint actuators, and the experimental performance of the integral sliding mode observer is evaluated by comparing the predefined disturbance $\boldsymbol{d}_{\mathrm{ext}}$ and its estimation $\hat{\boldsymbol{d}}_{\mathrm{ext}}$.

The experiment configurations are as follows. The manipulator platform is actuated by 3 Maxon torque motors on the joints with a turn ratio of 1:100. The actuators are installed in parallel along the axes, such that the robot moves in the horizontal plane and gravity is ignored. The incremental encoders offer the joint position measurement with a resolution of 2000. The sensors and actuators are connected with the computer using a PCI communication card. The Maxon driver is used to communicate between the executable and the robot. The executable of the algorithm is created by MATLAB 2017a in Ubuntu 14.04 LTS, with the first order Euler solver at the sampling rate of 1 kHz, and runs for 70 s. The dynamic model of the robot is well identified.

A. Estimation of Predefined Disturbances

In the first experiment, a trajectory tracking task is implemented on the robot platform. The desired trajectory $\boldsymbol{q}_d(t)$ is designed as

$$\boldsymbol{q}_d(t) = \left(1 - \cos\left(\frac{2\pi}{5}t\right)\right)\boldsymbol{k}_{\mathrm{pos}},\ 5 < t \leqslant 65. \tag{53}$$

which is shown in Fig. (4). The PD controller in (51) is implemented to track the given trajectory (53).

During the motion of the manipulator, three different kinds of predefined disturbances $\boldsymbol{d}_{\mathrm{ext}}(t)$ are inserted to the robot joint command inputs to simulate the external force, such that the comparison can be made between the estimated contact force $\hat{\boldsymbol{d}}_{\mathrm{ext}}(t)$ and the original disturbance $\boldsymbol{d}_{\mathrm{ext}}(t)$. Respectively, the sinusoidal disturbance (also used in [3]), the square form disturbance (also used in [4], [30], [34]) and the triangle form disturbance (also used in [29]) are used in this experiment, since they all resemble the waveform of contact force in practice which is featured with large amplitudes, short time periods and summit-shape waveform. The specific formulations are as follows:

Disturbance 1. Sinusoidal waveform

$$\boldsymbol{d}_{\sin}(t) = \begin{cases} \sin\left(\frac{\pi}{2}(t-12.5)\right)\boldsymbol{k}_{\mathrm{dst}}, & 12.5 < t \leqslant 14.5, \\ 0, & \text{else}. \end{cases} \tag{54}$$

Disturbance 2. Square waveform

$$\boldsymbol{d}_{\mathrm{sqr}}(t) = \begin{cases} \boldsymbol{k}_{\mathrm{dst}}, & 12.5 < t \leqslant 14.5, \\ 0, & \text{else}. \end{cases} \tag{55}$$

Disturbance 3. Triangle waveform

$$\boldsymbol{d}_{\mathrm{trg}}(t) = \begin{cases} (t-12.5)\boldsymbol{k}_{\mathrm{dst}}, & 12.5 < t \leqslant 13.5, \\ (-t+14.5)\boldsymbol{k}_{\mathrm{dst}}, & 13.5 < t \leqslant 14.5, \\ 0, & \text{else}. \end{cases} \tag{56}$$

An integral sliding mode observer in (16) is implemented on the robot platform with the same parameter selection as in Tab V. The evaluation of the estimation results are as follows.

Fig. (5) shows the estimation results of the first robot joint with the sinusoidal disturbance from (54). Similar to the simulation results, the precise estimation $\hat{\boldsymbol{d}}_{\mathrm{ext}}(t)$ and $\dot{\hat{\boldsymbol{q}}}(t)$ of the disturbance $\boldsymbol{d}_{\mathrm{ext}}(t)$ and velocity $\dot{\boldsymbol{q}}(t)$ of the system can be respectively seen in Fig. (5a) and Fig. (5b). In Fig. (5c), it is obvious that the switching function remains in the region $\|\boldsymbol{s}(t)\| < 2 \times 10^{-4}$. These results have confirmed the robustness of the integral sliding mode observer.

The estimation results of the square form disturbance and the triangle form disturbance are shown in Fig. (6) and Fig. (7). Apart from the similar arguments to the above, Fig. (6b) especially shows the precise tracking of joint velocity even with high bandwidth signal perturbations (e.g. in 12.5 s and 14.5 s) which are caused by the jumps on the system disturbance. Thus again, the high-bandwidth and robustness of this observer are confirmed.

B. Estimation of Contact Force

In this experiment, we investigate the performance of the integral sliding mode observer which estimates the contact forces between the robot and the environment. To make a comparison, a JR3 force sensor (see Fig. (8a)) is installed to the end-effector of the manipulator to measure the contact forces, which provides the measurement as a wrench form in Cartesian space. A plastic attachment is fixed with the JR3 force sensor with a spherical appendix (see Fig. (8b)) to guarantee a firm and steady contact. A sponge fixed to a stick holder (see Fig. (8b)) is used to make contacts with the spherical appendix instead of human hands. The desired trajectory is given as (53) and the PD controller in (51) is used. The configuration of the integral sliding mode observer is the same as the previous experiment.

During the motion of the manipulator, several contacts are made to the spherical appendix on the end-effector using the

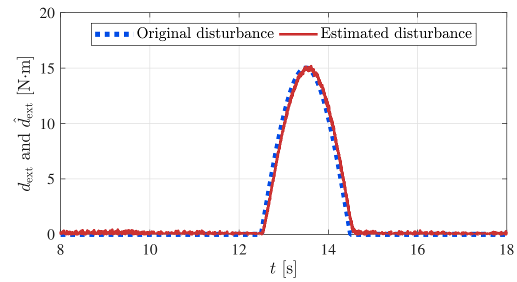

(a) The disturbance $\hat{d}_{\mathrm{ext}}(t)$ and its estimation $\hat{d}_{\mathrm{ext}}(t)$ of the first joint.

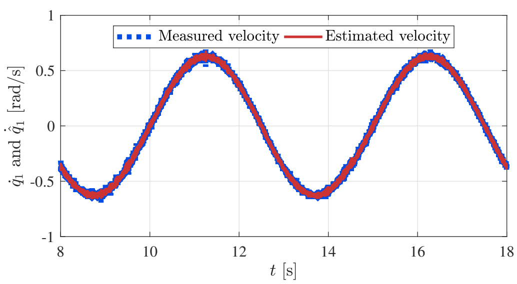

(b) The velocity $\dot{q}_1(t)$ and its estimation $\hat{\dot{q}}_1(t)$ of the first joint.

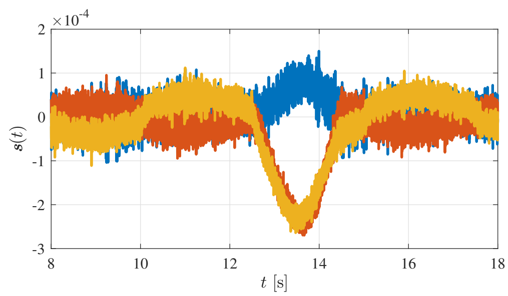

(c) The switching function $\boldsymbol{s}(t)$ of the observer.

Fig. 5. The results of observer for sinusoidal disturbance.

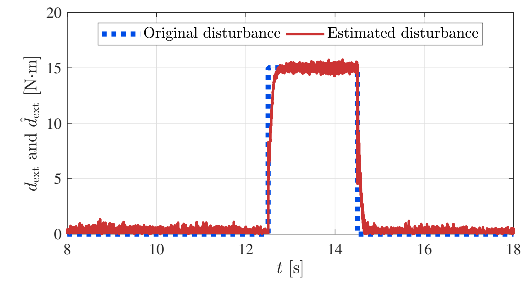

(a) The disturbance $\hat{d}_{\mathrm{ext}}(t)$ and its estimation $\hat{d}_{\mathrm{ext}}(t)$ of the first joint.

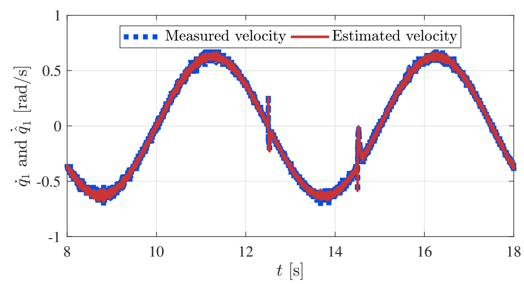

(b) The velocity $\dot{q}_1$ and its estimation $\hat{\dot{q}}_1(t)$ of the first joint.

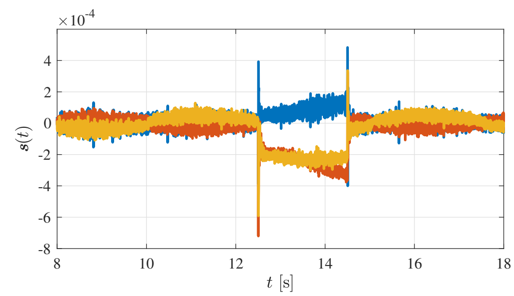

(c) The switching function $\boldsymbol{s}(t)$ of the observer.

Fig. 6. The results of observer for square form disturbance

sponge to simulate the robot-environment contacts in a robot task. The occurrence time instances of the manual contacts are approximately 37 s, 42 s, 47 s, 52 s, 57 s, and 62 s. At the same time, the contact force is measured and recorded. Note that the measurement of JR3 is in the form of a wrench $\boldsymbol{F}_m \in \mathbb{R}^6$ in the task coordinate, whereas the estimated torque $\hat{\boldsymbol{d}}_{\mathrm{ext}}$ is in the joint coordinate. Therefore, we transform the measured contact wrench into the joint space coordinate by $\boldsymbol{\tau}_m = \boldsymbol{J}^T(\boldsymbol{q})\boldsymbol{T}(\boldsymbol{q})\boldsymbol{F}_m$, where the measured external torque $\boldsymbol{\tau}_m$ denotes the reflection of $\boldsymbol{F}_m$ in the joint coordinate, $\boldsymbol{J}(\boldsymbol{q})$ is the Jacobian matrix and $\boldsymbol{T}(\boldsymbol{q})$ is the coordinate transformation from the task coordinate to the base coordinate. The comparison between the measured external torque $\boldsymbol{\tau}_m$ and the estimated external torque $\hat{\boldsymbol{d}}_{\mathrm{ext}}$ is shown in Fig. (9).

The results have shown that the estimation $\hat{\boldsymbol{d}}_{\mathrm{ext}}$ by the observer is very close to the measured external torque $\boldsymbol{\tau}_m$ by JR3 torque sensor. Note that the waveform of the external torques possess similar features to the predefined disturbances in (54), (55) and (56). This confirms the estimation precision and bandwidth of the integral sliding mode observer in practical applications.

C. Application Example: Sensorless Admittance Control

The precise, high-bandwidth and robust estimation performance of the integral sliding mode observer confirmed by the above simulation and experiments reveals its potential application to safe human robot collaborations, which is investigated in this section by implementing a force-sensor-less admittance controller as an example. An admittance controller is an important component in the HRI safety framework. By modifying the reference trajectory according to the external force feedback, the robot can compliantly react to the interactive forces, such that an admittance featured motion is achieved. Usually an external force sensor, such as the JR3 torque sensor, is needed to implement an admittance controller, whereas here we use the estimated external torque $\hat{\boldsymbol{d}}_{\mathrm{ext}}$ instead of the measured torque $\boldsymbol{\tau}_m$. Thus the admittance controller in this experiment is designed as follows

$$\boldsymbol{\tau} = \hat{\boldsymbol{M}}(\boldsymbol{q})\left(\ddot{\boldsymbol{q}}_r + \boldsymbol{K}_D\dot{\boldsymbol{e}}_r + \boldsymbol{K}_P\boldsymbol{e}_r\right) + \hat{\boldsymbol{C}}(\boldsymbol{q},\dot{\boldsymbol{q}})\dot{\boldsymbol{q}} + \hat{\boldsymbol{F}}(\dot{\boldsymbol{q}}),$$

where $\boldsymbol{q}_r$ and $\dot{\boldsymbol{q}}_r$ are respectively the reference position and velocity of the robot in the joint space, $\boldsymbol{e}_r = \boldsymbol{q}_r - \boldsymbol{q}$ is the deviation between the reference position and the current

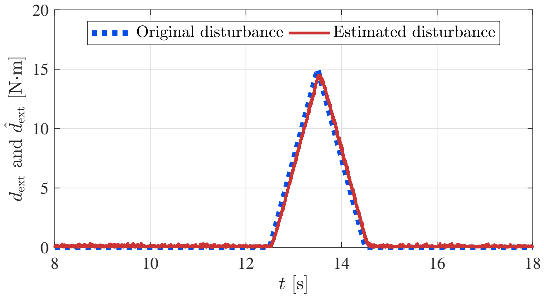

(a) The disturbance $\hat{d}_{\mathrm{ext}}(t)$ and its estimation $\hat{d}_{\mathrm{ext}}(t)$ of the first joint.

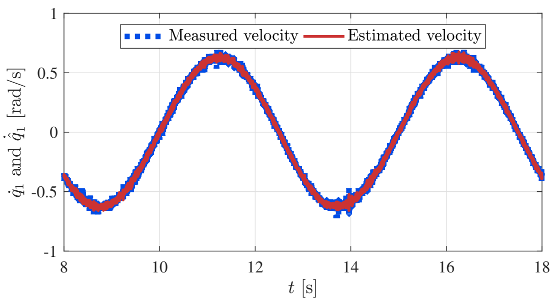

(b) The velocity $\dot{q}_1$ and its estimation $\hat{\dot{q}}_1(t)$ of the first joint.

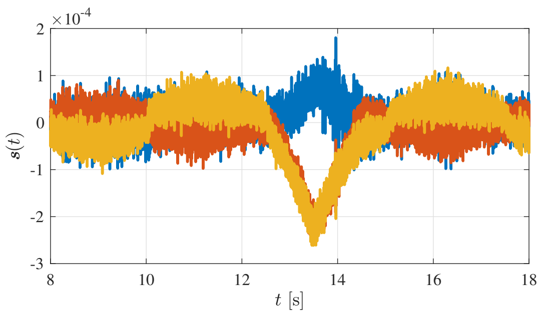

(c) The switching function $\boldsymbol{s}(t)$ of the observer.

Fig. 7. The results of observer for triangle form disturbance

(a)

(b)

Fig. 8. The contact devices and the JR3 force sensor

position, $\boldsymbol{K}_D$ and $\boldsymbol{K}_P$ are the same as in (51). The reference trajectory $\boldsymbol{q}_r$ is defined by

$$\dot{\boldsymbol{q}}_r = \dot{\boldsymbol{q}}_d + \boldsymbol{K}_d^{-1}\left(\boldsymbol{K}_p(\boldsymbol{q}_d - \boldsymbol{q}_r) + \hat{\boldsymbol{d}}_{\mathrm{ext}}\right), \tag{57}$$

where $\boldsymbol{K}_p = 50\boldsymbol{I}_3$ and $\boldsymbol{K}_d = 50\boldsymbol{I}_3$ respectively define the stiffness and damp of the admittance behavior. Note that

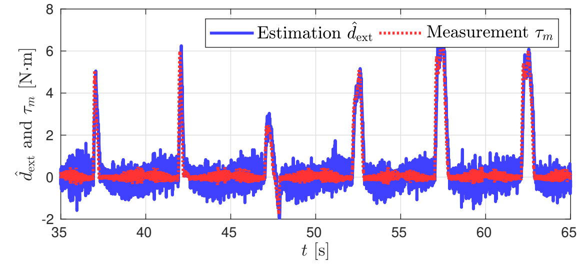

Fig. 9. The comparison between the estimation of the observer and the measurement by JR3 force sensor (on the first joint).

different from the simulation and the experiments above, the estimated disturbance $\hat{\boldsymbol{d}}_{\mathrm{ext}}$ is applied to the closed-loop control, see (57). The motion of the robot with this force-sensor-less admittance controller is shown in Fig. (10). Initially, the robot stays in a static position (see Fig. (10a)). When an object makes a contact with the end-effector (see Fig. (10b)), an admittance reaction behaviour is achieved (see Fig. (10c)). After the contact vanishes, the robot returns to the original configuration. Note that due to the approximation from (24), the filter (25) and the boundary layer techniques (50), $\hat{\boldsymbol{d}}_{\mathrm{ext}}$ is not exactly equal to $\boldsymbol{d}_{\mathrm{ext}}$. As a result, the closed-loop stability of the admittance controller does not hold for all possible values of K_d and K_p as in (57). Large values of τ and the boundary layers may lead to small feasible sets of control parameters K_d and K_p.

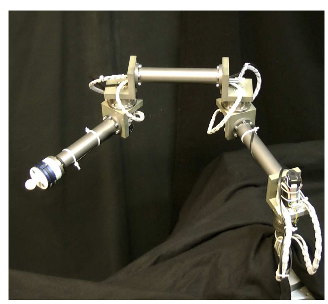

(a)

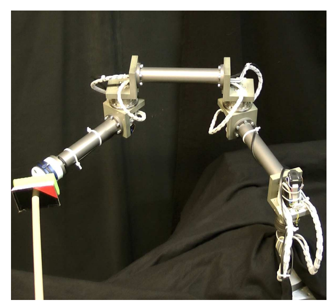

(b)

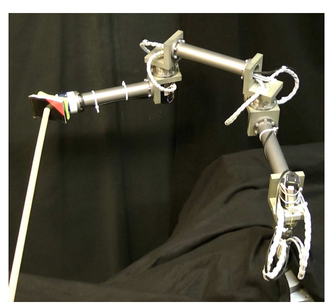

(c)

(d)

Fig. 10. The reactive motion of force-sensor-less admittance controller

As shown in the example demonstration above, the force-sensor-less admittance controller reveals an expected compliance behavior when physical contact is exerted on the end-effector, which justifies the applicability of the integral sliding mode observer to practical HRC scenarios. Thus, a safe compliance controller can be designed without expensive force sensory devices. The disadvantage is, however, the resulting control precision is inferior to the control schemes using force sensors due to applying the filter and boundary layer techniques. Therefore, this force-sensor-less application is suitable to the low-cost robot platforms which do not have strict requirements on the force control precision.

VI. Conclusion

A novel integral sliding mode observer is proposed for Euler-Lagrangian systems and applied to a robot platform. In the mathematical point of view, this observer requires fewer assumptions. An integral sliding mode is applied to achieve enhanced invariance. Thus robust velocity and disturbance estimations are obtained by this observer at the same time. Numerical simulation and experiments have shown the high precision, bandwidth, and robustness of this novel method. The experimental comparison with sensory measurements reveals its possibility to replace a real force sensor in practice. The implementation of a force-sensor-less admittance controller lights up the ambition to achieve a sensor-free and low-cost safety framework for human-friendly collaborative robots. Considering the insufficiency of the rigid robot models, future work will be dedicated to improving the performance of this disturbance observer with joint elastics.

Appendix A

This appendix provides the derivation of the error dynamics (20) of the proposed observer (16) and estimate the boundary of the system uncertainty h_O in Assumption 3. By combining the observer dynamics (16) and the original system (8), we have

$$\begin{aligned}\dot{\boldsymbol{e}}_2 =& \boldsymbol{M}^{-1}\boldsymbol{C}(\boldsymbol{x}_1,\boldsymbol{x}_2)\boldsymbol{x}_2 - \hat{\boldsymbol{M}}^{-1}\hat{\boldsymbol{C}}(\boldsymbol{x}_1,\hat{\boldsymbol{x}}_2)\hat{\boldsymbol{x}}_2\\ &+ \boldsymbol{M}^{-1}\boldsymbol{G} - \hat{\boldsymbol{M}}^{-1}\hat{\boldsymbol{G}} + \boldsymbol{M}^{-1}\boldsymbol{F}(\boldsymbol{x}_2) - \hat{\boldsymbol{M}}^{-1}\hat{\boldsymbol{F}}(\hat{\boldsymbol{x}}_2)\\ &- \boldsymbol{M}^{-1}\boldsymbol{\tau} + \hat{\boldsymbol{M}}^{-1}\boldsymbol{\tau} - \boldsymbol{d}(\boldsymbol{x}_1,t) + \boldsymbol{\Gamma}_2\boldsymbol{u}_1 + \boldsymbol{u}_2,\end{aligned} \tag{58}$$

where $\boldsymbol{x}_1$ is omitted in the inertia matrices $\boldsymbol{M}$ and $\hat{\boldsymbol{M}}$ and the gravity matrices $\boldsymbol{G}$ and $\hat{\boldsymbol{G}}$. Here we define the model deviations as

$$\begin{aligned}&\tilde{\boldsymbol{C}}(\boldsymbol{x}_1,\hat{\boldsymbol{x}}_2) = \boldsymbol{C}(\boldsymbol{x}_1,\hat{\boldsymbol{x}}_2) - \hat{\boldsymbol{C}}(\boldsymbol{x}_1,\hat{\boldsymbol{x}}_2),\\ &\tilde{\boldsymbol{G}} = \boldsymbol{G} - \hat{\boldsymbol{G}},\ \ \tilde{\boldsymbol{F}} = \boldsymbol{F}(\boldsymbol{x}_2) - \hat{\boldsymbol{F}}(\hat{\boldsymbol{x}}_2).\end{aligned}$$

Therefore, (58) results in

$$\begin{aligned}\dot{\boldsymbol{e}}_2 =& \Big(\boldsymbol{M}^{-1} - \hat{\boldsymbol{M}}^{-1}\Big)\Big(\hat{\boldsymbol{C}}(\boldsymbol{x}_1,\hat{\boldsymbol{x}}_2)\hat{\boldsymbol{x}}_2 + \hat{\boldsymbol{G}} + \hat{\boldsymbol{F}}(\hat{\boldsymbol{x}}_2) - \boldsymbol{\tau}\Big)\\ &- \boldsymbol{M}^{-1}\Big(\hat{\boldsymbol{C}}(\boldsymbol{x}_1,\hat{\boldsymbol{x}}_2)\hat{\boldsymbol{x}}_2 - \boldsymbol{C}(\boldsymbol{x}_1,\boldsymbol{x}_2)\boldsymbol{x}_2 + \tilde{\boldsymbol{G}} + \tilde{\boldsymbol{F}}\Big)\\ &- \boldsymbol{d} + \boldsymbol{\Gamma}_2\boldsymbol{u}_1 + \boldsymbol{u}_2.\end{aligned} \tag{59}$$

Considering

$$\begin{aligned}&\hat{\boldsymbol{C}}(\boldsymbol{x}_1,\hat{\boldsymbol{x}}_2)\hat{\boldsymbol{x}}_2 - \boldsymbol{C}(\boldsymbol{x}_1,\boldsymbol{x}_2)\boldsymbol{x}_2 = \boldsymbol{C}(\boldsymbol{x}_1,\hat{\boldsymbol{x}}_2)\hat{\boldsymbol{x}}_2\\ &\quad - \boldsymbol{C}(\boldsymbol{x}_1,\boldsymbol{x}_2)\boldsymbol{x}_2 + \hat{\boldsymbol{C}}(\boldsymbol{x}_1,\hat{\boldsymbol{x}}_2)\hat{\boldsymbol{x}}_2 - \boldsymbol{C}(\boldsymbol{x}_1,\hat{\boldsymbol{x}}_2)\hat{\boldsymbol{x}}_2\\ &= \boldsymbol{C}(\boldsymbol{x}_1,\hat{\boldsymbol{x}}_2)\hat{\boldsymbol{x}}_2 - \boldsymbol{C}(\boldsymbol{x}_1,\boldsymbol{x}_2)\boldsymbol{x}_2 + \tilde{\boldsymbol{C}}(\boldsymbol{x}_1,\hat{\boldsymbol{x}}_2)\hat{\boldsymbol{x}}_2\\ &= \boldsymbol{C}(\boldsymbol{x}_1,\hat{\boldsymbol{x}}_2)\hat{\boldsymbol{x}}_2 - \boldsymbol{C}(\boldsymbol{x}_1,\hat{\boldsymbol{x}}_2)\boldsymbol{x}_2 + \tilde{\boldsymbol{C}}(\boldsymbol{x}_1,\hat{\boldsymbol{x}}_2)\hat{\boldsymbol{x}}_2,\\ &\quad + \boldsymbol{C}(\boldsymbol{x}_1,\hat{\boldsymbol{x}}_2)\boldsymbol{x}_2 - \boldsymbol{C}(\boldsymbol{x}_1,\boldsymbol{x}_2)\boldsymbol{x}_2\end{aligned} \tag{60}$$

and by substituting $\boldsymbol{C}(\boldsymbol{x}_1,\hat{\boldsymbol{x}}_2)\boldsymbol{x}_2 = \boldsymbol{C}(\boldsymbol{x}_1,\boldsymbol{x}_2)\hat{\boldsymbol{x}}_2$, which is supported by Property 5, to (60), we have

$$\begin{aligned}&\hat{\boldsymbol{C}}(\boldsymbol{x}_1,\hat{\boldsymbol{x}}_2)\hat{\boldsymbol{x}}_2 - \boldsymbol{C}(\boldsymbol{x}_1,\boldsymbol{x}_2)\boldsymbol{x}_2\\ &= \boldsymbol{C}(\boldsymbol{x}_1,\hat{\boldsymbol{x}}_2)\hat{\boldsymbol{x}}_2 - \boldsymbol{C}(\boldsymbol{x}_1,\hat{\boldsymbol{x}}_2)\boldsymbol{x}_2 + \tilde{\boldsymbol{C}}(\boldsymbol{x}_1,\hat{\boldsymbol{x}}_2)\hat{\boldsymbol{x}}_2,\\ &\quad + \boldsymbol{C}(\boldsymbol{x}_1,\boldsymbol{x}_2)\hat{\boldsymbol{x}}_2 - \boldsymbol{C}(\boldsymbol{x}_1,\boldsymbol{x}_2)\boldsymbol{x}_2\\ &= \boldsymbol{C}(\boldsymbol{x}_1,\hat{\boldsymbol{x}}_2)\boldsymbol{e}_2 + \tilde{\boldsymbol{C}}(\boldsymbol{x}_1,\hat{\boldsymbol{x}}_2)\hat{\boldsymbol{x}}_2 + \boldsymbol{C}(\boldsymbol{x}_1,\boldsymbol{x}_2)\boldsymbol{e}_2.\end{aligned} \tag{61}$$

Therefore, substituting (61) to (59) and compare with (20), we figure out the expression of $\boldsymbol{h}(\boldsymbol{x}_1,\hat{\boldsymbol{x}}_2)$ as

$$\begin{aligned}\boldsymbol{h}(\boldsymbol{x}_1,\hat{\boldsymbol{x}}_2) =& \boldsymbol{M}^{-1}\Big(\tilde{\boldsymbol{C}}(\boldsymbol{x}_1,\hat{\boldsymbol{x}}_2)\hat{\boldsymbol{x}}_2 + \tilde{\boldsymbol{G}} + \tilde{\boldsymbol{F}}\Big)\\ &+ \Big(\hat{\boldsymbol{M}}^{-1} - \boldsymbol{M}^{-1}\Big)\Big(\hat{\boldsymbol{C}}(\boldsymbol{x}_1,\hat{\boldsymbol{x}}_2)\hat{\boldsymbol{x}}_2 + \hat{\boldsymbol{G}} + \hat{\boldsymbol{F}}(\hat{\boldsymbol{x}}_2) - \boldsymbol{\tau}\Big).\end{aligned} \tag{62}$$

Note that the identified parametric matrices $\hat{\boldsymbol{M}}$, $\hat{\boldsymbol{C}}(\boldsymbol{x}_1,\hat{\boldsymbol{x}}_2)$, $\hat{\boldsymbol{G}}(\boldsymbol{x}_1)$ and $\hat{\boldsymbol{F}}(\hat{\boldsymbol{x}}_2)$ do not depend on the modeling deviations. Therefore, (62) indicates that the system uncertainty $\boldsymbol{h}(\boldsymbol{x}_1,\hat{\boldsymbol{x}}_2)$ is linearly dependent on the deviations $\tilde{\boldsymbol{C}}(\boldsymbol{x}_1,\hat{\boldsymbol{x}}_2)$, $\tilde{\boldsymbol{G}}$ and $\tilde{\boldsymbol{F}}$. By applying precise system identification procedures, the uncertainty boundary $\|\boldsymbol{h}(\boldsymbol{x}_1,\hat{\boldsymbol{x}}_2)\|$ can be reduced.

References

[1] J.-W. Zhu, G.-H. Yang, H. Wang, and F. Wang, "Fault Estimation for a Class of Nonlinear Systems Based on Intermediate Estimator," *IEEE Transactions on Automatic Control*, vol. 61, no. 9, pp. 2518–2524, 2016.

[2] C. P. Tan and C. Edwards, "Sliding mode observers for detection and reconstruction of sensor faults," *Automatica*, vol. 38, no. 10, pp. 1815–1821, 2002.

[3] B. Jiang, M. Staroswiecki, and V. Cocquempot, "Fault accommodation for nonlinear dynamic systems," *IEEE Transactions on Automatic Control*, vol. 51, pp. 1578–1583, 2006.

[4] D. Brambilla, L. M. Capisani, A. Ferrara, and P. Pisu, "Fault detection for robot manipulators via second-order sliding modes," *IEEE Transactions on Industrial Electronics*, vol. 55, no. 11, pp. 3954–3963, 2008.

[5] A. De Santis, B. Siciliano, A. De Luca, and A. Bicchi, "An atlas of physical human-robot interaction," *Mechanism and Machine Theory*, vol. 43, no. 3, pp. 253–270, 2008.

[6] Y. Zhang and Q. Xu, "Adaptive Sliding Mode Control With Parameter Estimation and Kalman Filter for Precision Motion Control of a Piezo-Driven Microgripper," *IEEE Transactions on Control Systems Technology*, vol. 25, no. 2, pp. 728–735, 2016.

[7] Z. Gao and S. X. Ding, "State and disturbance estimator for time-delay systems with application to fault estimation and signal compensation," *IEEE Transactions on Signal Processing*, vol. 55, no. 12, pp. 5541–5551, 2007.

[8] C. Wang, L. Quan, Z. Jiao, and S. Zhang, "Nonlinear Adaptive Control of Hydraulic System With Observing and Compensating," *IEEE Transactions on Control Systems Technology*, vol. 26, no. 3, pp. 927–938, 2017.

[9] A. De Luca and R. Mattone, "Actuator failure detection and isolation using generalized momenta," in *IEEE International Conference on Robotics and Automation*, vol. 1, 2003, pp. 634–639.

[10] S. Haddadin, A. Albu-Schäffer, and G. Hirzinger, "Safety evaluation of physical human-robot interaction via crash-testing." in *Robotics: Science and Systems*, vol. 3, 2007, pp. 217–224.

[11] M. Geravand, F. Flacco, and A. De Luca, "Human-robot physical interaction and collaboration using an industrial robot with a closed control architecture," in *IEEE International Conference on Robotics and Automation*, 2013, pp. 4000–4007.

[12] M. A. Goodrich and A. C. Schultz, "Human-robot interaction: a survey," *Foundations and trends in human-computer interaction*, vol. 1, no. 3, pp. 203–275, 2007.

[13] T. Fong, I. Nourbakhsh, and K. Dautenhahn, "A survey of socially interactive robots," *Robotics and autonomous systems*, vol. 42, no. 3-4, pp. 143–166, 2003.

[14] A. Bauer, D. Wollherr, and M. Buss, "Human-robot collaboration: a survey," *International Journal of Humanoid Robotics*, vol. 5, no. 01, pp. 47–66, 2008.

[15] M. Bohm, J. U. Pott, M. Kurster, O. Sawodny, D. Defrere, and P. Hinz, "Delay Compensation for Real Time Disturbance Estimation at Extremely Large Telescopes," *IEEE Transactions on Control Systems Technology*, vol. 25, no. 4, pp. 1384–1393, 2017.
[16] J. Qin, H. Gao, and W. X. Zheng, "Fault-tolerant cooperative tracking control via integral sliding mode control technique," *IEEE/ASME Tansactions on Mechatronics*, vol. 23, no. 1, pp. 342–351, 2018.
[17] S. Pigg and M. Bodson, "Adaptive algorithms for the rejection of sinusoidal disturbances acting on unknown plants," *IEEE Transactions on Control Systems Technology*, vol. 18, no. 4, pp. 822–836, 2010.
[18] M. Van, "An Enhanced Robust Fault Tolerant Control Based on an Adaptive Fuzzy PID- Nonsingular Fast Terminal Sliding Mode Control for Uncertain Nonlinear Systems," *IEEE/ASME Transactions on Mechatronics*, vol. 23, no. 3, pp. 1362–1371, 2018.
[19] Y. Wan and T. Keviczky, "Real-Time Fault-Tolerant Moving Horizon Air Data Estimation for the RECONFIGURE Benchmark," *IEEE Transactions on Control Systems Technology*, pp. 1–15, 2018.
[20] A. AlbuSchäffer, S. Haddadin, C. Ott, A. Stemmer, T. Wimböck, and G. Hirzinger, "The DLR lightweight robot: design and control concepts for robots in human environments," *Industrial Robot: An International Journal*, vol. 34, no. 5, pp. 376–385, 2007.
[21] J. J. Gertler, "Survey of Model-Based Failure Detection and Isolation in Complex Plants," *IEEE Control Systems Magazine*, vol. 8, no. 6, pp. 3–11, 1988.
[22] F. Flacco and A. De Luca, "Safe physical human-robot collaboration," in *IEEE International Conference on Intelligent Robots and Systems*, 2013, p. 2072.
[23] M. S. Khireddine, K. Chafaa, N. Slimane, and A. Boutarfa, "Sensor and actuator fault diagnosis based on soft computing techniques," *Journal of Intelligent Systems*, vol. 24, no. 1, pp. 1–21, 2015.
[24] W. H. Chen, D. J. Ballance, P. J. Gawthrop, and J. O'Reilly, "A nonlinear disturbance observer for robotic manipulators," *IEEE Transactions on Industrial Electronics*, vol. 47, no. 4, pp. 932–938, 2000.
[25] W. Chen and M. Saif, "Robust fault detection and isolation in constrained nonlinear systems via a second order sliding mode observer," *IFAC Proceedings Volumes*, vol. 35, no. 1, pp. 269–274, 2002.
[26] A. Colome, D. Pardo, G. Alenya, and C. Torras, "External force estimation during compliant robot manipulation," in *Proceedings - IEEE International Conference on Robotics and Automation*, 2013, pp. 3535–3540.
[27] F. Caccavale and I. Walker, "Observer-based fault detection for robot manipulators," in *Proceedings of International Conference on Robotics and Automation*, vol. 4, no. April, 1997, pp. 2881–2887.
[28] C. Canudas de Wit and J. J. E. Slotine, "Sliding observers for robot manipulators," *Automatica*, vol. 27, no. 5, pp. 859–864, 1991.
[29] C. Edwards, S. K. Spurgeon, and R. J. Patton, "Sliding mode observers for fault detection and isolation," *Automatica*, vol. 36, no. 4, pp. 541–553, 2000.
[30] L. M. Capisani, A. Ferrara, A. de Loza, and L. M. Fridman, "Manipulator Fault Diagnosis via Higher Order Sliding-Mode Observers," *IEEE Transactions on Industrial Electronics*, vol. 59, no. 10, pp. 3979–3986, 2012.
[31] Y. Sun, Z. Zhang, M. Leibold, R. Hayat, D. Wollherr, and M. Buss, "Protective control for robot manipulator by sliding mode based disturbance reconstruction approach," in *2017 IEEE International Conference on Advanced Intelligent Mechatronics (AIM)*, 2017, pp. 1015–1022.
[32] B. Bona and M. Indri, "Analysis and implementation of observers for robotic manipulators," *Proceedings 1998 IEEE International Conference on Robotics and Automation Cat No98CH36146*, vol. 4, no. May, pp. 3006–3011, 1998.
[33] W. Kim, D. Shin, D. Won, and C. C. Chung, "Disturbance-observer-based position tracking controller in the presence of biased sinusoidal disturbance for electrohydraulic actuators," *IEEE Transactions on Control Systems Technology*, vol. 21, no. 6, pp. 2290–2298, 2013.
[34] W. H. Chen, "Disturbance Observer Based Control for Nonlinear Systems," *IEEE/ASME Transactions on Mechatronics*, vol. 9, no. 4, pp. 706–710, 2004.
[35] V. I. Utkin and H.-C. Chang, "Sliding mode control on electro-mechanical systems," pp. 451–473, 2002.
[36] T. Floquet and J. P. Barbot, "Super twisting algorithm-based step-by-step sliding mode observers for nonlinear systems with unknown inputs," *International Journal of Systems Science*, vol. 38, no. 10, pp. 803–815, 2007.
[37] C. Edwards and S. K. Spurgeon, "Sliding mode stabilization of uncertain systems using only output information," *International Journal of Control*, vol. 62, no. 5, pp. 1129–1144, 1995.
[38] V. Utkin and J. S. J. Shi, "Integral sliding mode in systems operating under uncertainty conditions," *Proceedings of 35th IEEE Conference on Decision and Control*, vol. 4, no. December, pp. 1–6, 1996.
[39] Y. Niu, D. W. C. Ho, and J. Lam, "Robust integral sliding mode control for uncertain stochastic systems with time-varying delay," *Automatica*, vol. 41, no. 5, pp. 873 – 880, 2005.
[40] S. Laghrouche, F. Plestan, and A. Glumineau, "Higher order sliding mode control based on integral sliding mode," *Automatica*, vol. 43, no. 3, pp. 531 – 537, 2007.
[41] G. P. Incremona, A. Ferrara, and L. Magni, "Mpc for robot manipulators with integral sliding modes generation," *IEEE/ASME Transactions on Mechatronics*, vol. 22, no. 3, pp. 1299–1307, 2017.
[42] M. Rubagotti, A. Estrada, F. Castaños, A. Ferrara, and L. Fridman, "Integral sliding mode control for nonlinear systems with matched and unmatched perturbations," *IEEE Transactions on Automatic Control*, vol. 56, no. 11, pp. 2699–2704, 2011.
[43] J.-X. Xu, Z.-Q. Guo, and T. H. Lee, "Design and implementation of integral sliding-mode control on an underactuated two-wheeled mobile robot," *IEEE Transactions on industrial electronics*, vol. 61, no. 7, pp. 3671–3681, 2014.
[44] B. Draenovi, "The invariance conditions in variable structure systems," *Automatica*, vol. 5, no. 3, pp. 287 – 295, 1969.
[45] A. De Luca, A. Albu-Schäffer, S. Haddadin, and G. Hirzinger, "Collision detection and safe reaction with the DLR-III lightweight manipulator arm," in *IEEE International Conference on Intelligent Robots and Systems*, 2006, pp. 1623–1630.
[46] B. Siciliano and O. Khatib, *Handbook of Robotics*. Springer, 2007.
[47] H. K. Khalil, "Nonlinear systems," *Upper Saddle River*, 2002.

Zengjie Zhang received his Bachelor and Master degrees from Harbin Institute of Technology, China, in 2013 and 2015 respectively. He is currently a Research Associate at the Chair of Automatic Control Engineering of the Technical University of Munich, Germany while pursuing the doctoral degree. His research interests include sliding mode control, fault detection and isolation and human-robot collaboration.

Marion Leibold received her Diploma degree in Applied Mathematics and her Ph.D. degree in Electrical Engineering from the Technical University of Munich, Germany, in 2002 and 2007, respectively. She is currently a Lecturer in the Chair of Automatic Control Engineering of the Technical University of Munich. Her research interests include hybrid dynamical systems, optimal control and legged robots.

Dirk Wollherr received the Diplom-Ingenieur degree and the Doctor of Engineering degree, both in electrical engineering, and the Habilitation degree from Technical University Munich, Germany, in 2000, 2005, and 2013, respectively. From 2001 to 2004, he was a Research Assistant with the Control Systems Group, Technische Universitt Berlin, Germany. In 2004, he was with the Yoshihiko Nakamura Laboratory, The University of Tokyo, Japan. Since 2014, he has been a Professor with the Chair of Automatic Control Engineering, Department of Electrical and Computer Engineering, Technical University Munich. His research interests include automatic control, robotics, autonomous mobile robots, humanrobot interaction, and humanoid walking.